FINAL REPORT

Modeling of Compton Scattering in Remote-Handled Waste Drum for Advanced Detector Program

(The Computational Models and Results of Simulations of Compton Scattering of 662keV Photons, Developed for Organic Debris Waste in a Drum Container and for Standard Drum Overpack)

Final Report (rev. 0)

Prepared by:

Bojan Petrovic (Bojan.Petrovic@gatech.edu)
Jordan McKillop (Jordan.McKillop@gatech.edu)
Georgia Institute of Technology
George W. Woodruff School of Mechanical Engineering
Nuclear and Radiological Engineering
771 Ferst Drive NW
Atlanta, GA 30332-0405

Performed Under:
Research Agreement R9233, PO# 4500270502

Submitted to:
Dr. Thomas V. Congedo (CongedTV@westinghouse.com)
Mr. Jerry A. Kyslinger (KyslinJA@westinghouse.com)
Westinghouse Electric Company LLC
Science and Technology Department
1344 Beulah Road
Pittsburgh, PA 15235-5083

September, 2008

(This page intentionally left blank)

EXECUTIVE SUMMARY

Disposal of remote-handled (RH) transuranic (TRU) waste is currently limited due to inability to fully characterize its properties (e.g., radiological and RCRA content) as required for disposal. The usefulness of established non-destructive evaluation methods by gamma-ray characterization is hindered by Compton scattering continuum in waste gamma-ray spectra.

The reported research is part of a larger multi-organization (Idaho National Laboratory, University of Florida, Westinghouse Electric Company LLC, Georgia Institute of Technology) multi-year project aimed at ultimately developing a novel detection system with Compton suppression combined with advanced data unfolding methods, that would enable significant improvement in non-destructive characterization via gamma-ray spectra. The specific work reported here relates only to a small portion of the overall efforts, i.e., a six-month research performed at the Georgia Institute of Technology, March-September 2008. The work was funded under the Prime Contract Number 00024953 from Bechtel BWXT Idaho LLC (now known as Battelle Energy Alliance LLC) to the University of Florida, Subcontract Number UF-EIES-0608003-WEC between UFL and Westinghouse, and the Research Agreement R9233 between Westinghouse and Georgia Institute of Technology.

The performed work addresses the Compton scattering in the waste matrix itself. The related topics of subsequent Compton scattering in the detector, Compton suppression, and unfolding algorithms were outside the scope of this study, and partly addressed in the work performed by other organizations.

In this study, organic waste in 55-gallon drum was considered, with or without an overpack. The reference source was defined to be ^{137}Cs; additionally, ^{60}Co was considered. The “reference case” or “base case” was established, with a representative (best estimate) waste matrix density and composition and the source centered in the drum. A number of “branch cases” were defined where a single or several parameters of the reference case were modified (such as the waste matrix density, source position, etc.), within a realistic range, to investigate their impact on the results.

The objective was to evaluate gamma spectra resulting from a mono-energetic gamma source of 662 keV, affected by Compton scattering within the waste drum, as observed outside the waste drum. Therefore, MCNP models were developed and Monte Carlo simulations performed for about 30 considered cases. The simulations were performed on an 8-CPU Dell Linux workstation. Due to the relative simplicity of the model and moderate attenuation between the source and selected locations outside the drum, it was possible to generate detailed results (with spectra energy bins of 1.33 keV width) with good statistics (statistical uncertainty at 1-sigma level typically of the order of a percent) within acceptable CPU times, of the order of an hour per simulation.

The leakage gamma spectra outside the drum were obtained at three selected locations, two of them corresponding to the source axial elevation plane, but one closer and one farther away from the drum, while the third one was close to the drum but off the source plane. The detailed raw results spectra) were extracted and saved for further post-processing, and are documented graphically within this report.

The impact of the Compton scattering within the waste on the spectrum shape, magnitude, and specific features was investigated. The ratio of the unscattered-to-scattered gammas, i.e., peak to total Compton was used as a representative single factor. The most relevant finding are summarized below.

The impact of the waste matrix density and composition was evaluated. The results essentially depend primarily on the matrix bulk density (g/cm^3) and do not differentiate much between the elements such as C, O, and N. Therefore, the best-estimate waste matrix composition is suitable for most analyses, i.e., for a wide variability in the waste matrix composition.

The density effect was further investigated. By subdividing the collided area into two portions, above and below the energy corresponding to backscatter at 180 degrees, and looking at the ration of these two subregions, provides a new parameter sensitive to the density change, which is expected to help in the future unfolding algorithm development.

The overpack was assumed to consist of 3.5" of steel. It reduces the uncollided photon flux by about two orders of magnitude and the collided one by one order of magnitude. It also masks/smears most of the spectral features, thus making unfolding of any information related to within-drum position significantly more difficult.

In another "branch" study, a radially off-center radiation source was assumed. It was demonstrated that using multiple detectors, for example a close and a far detector, interfering effects of the matrix density and source position may be resolved, and more accurate unfolding of the detector position may be accomplished.

Finally, to provide some bounds on the source energy impact, additional simulations were performed with a different source energy, corresponding to two main cobalt lines.

The presented results fully satisfy the requirements of the 6-month research agreement. However, these results are only the first step toward the overall long-term objective of using simulation results coupled with advanced unfolding algorithms to improve filtering out of the Compton-scattering component in the unfolding process. They provide a good basis for further research aimed to improving non-destructive gamma-ray based evaluation methods.

TABLE OF CONTENTS

(This page intentionally left blank)

1. Introduction

1.1 Background

A number of contact handled (CH) and remote handled (RH) waste drums are currently stored at various facilities awaiting the final disposal at WIPP. Disposal of remote-handled (RH) transuranic (TRU) waste is limited due to inability to adequately characterize its properties (e.g., radiological and RCRA content), which is a required to properly classify waste for disposal. Various active and passive non-destructive evaluation (NDE) methods are being tested and developed to enable effective and economical waste characterization. Among these, passive gamma-ray characterization methods are in principle well established and relatively simple, but their usefulness is hindered in waste RH by the large Compton scattering continuum background in waste gamma-ray spectra.

A multi-organization (Idaho National Laboratory, University of Florida, Westinghouse Electric Company LLC, Georgia Institute of Technology) multi-year project was initiated several years ago aimed at ultimately developing a novel detection system with Compton suppression combined with advanced data unfolding methods, that would enable significant improvement in non-destructive characterization via gamma-ray spectra. The specific work reported here relates only to a small portion of the overall efforts, i.e., a six-month research performed at the Georgia Institute of Technology, Mar-Sep 2008. The work was funded under the Prime Contract Number 00024953 from Bechtel BWXT Idaho LLC (now known as Battelle Energy Alliance LLC) to the University of Florida, Subcontract Number UF-EIES-0608003-WEC between UFL and Westinghouse, and the Research Agreement R9233 between Westinghouse and Georgia Institute of Technology.

The reported work addresses the first change of the original source spectrum, which occurs due to the Compton scattering in the waste matrix itself. The related topics of subsequent Compton scattering in the detector, possible Compton suppression by a detector system, and unfolding algorithms, were outside the scope of this study, and addressed in the work performed by other team organizations.

1.2 Objective

The objective was to evaluate gamma spectra resulting from a mono-energetic gamma source of 662 keV, affected by Compton scattering within the waste drum, as observed outside the waste drum. Specifically, the Statement of Work (SOW) defined the tasks as follows:

Task 1: Develop a computational model for Compton scattering of .662 MeV photons in organic debris waste and perform baseline numerical simulations

Transport theory models will be developed to enable simulation of the Compton scattering of gamma rays within the waste matrix and in the container. The reference

drum will be either a 55-gallon or a 30-gallon drum. Drum specifications will be provided by INL, or, in the absence of INL specifications, they will be prepared based on the information available in open literature. Studies of the cases with homogenous matrix and empty-drum will be performed.

<u>Task 2:</u> Develop a computation model for Compton scattering of .662 MeV photons in a standard overpack and perform numerical simulations.

The waste drum models will be extended to include a standard drum overpack. Simulations will be performed with and without the overpack, and, its impact examined by comparing the results.

Specifically, organic waste in 55-gallon drum was considered, empty or with homogeneous matrix, with or without a standard overpack. The reference source was defined to be ^{137}Cs as specified in SOW, but additionally ^{60}Co was added to allow evaluating the source energy impact. The "reference case" or "base case" was established, with a representative (best estimate) waste matrix density and composition. A number of "branch cases" were added beyond those strictly required by SOW, where a single or several parameters of the reference case were modified within a realistic range (such as the waste matrix density, source position, etc.), to investigate their impact on the results and obtain a better understanding of the potential use of these results in future spectra unfolding work.

2. Model Preparation

2.1 Methods, Analytic Tools and Hardware Used

The simulations were performed using Monte Carlo techniques. In the developed models, the particles were tallied at locations that represented detector positions as the objective was to get an estimate of photon spectrum at that position, rather than modeling the detector response.

The Monte Carlo N Particle Transport Code version 5, MCNP5 [1], created by Los Alamos National Laboratory under the auspices of the US Department of Energy, was used for all simulations.

This particular compilation of MCNP5 was compiled based on the latest release from the Radiation Safety Information Computational Center (RSICC) as of January 2008. The Intel Compiler Suite version 10.1 was used to build the executables with several optimization options selected at build time. The optimization flag was set to –O0 based on recommendations from building instructions. Higher levels of optimization cause failures during the testing portion of the building phase. The flag –xP was selected based on the processors in the system. The –openmp flag was used to active the built-in parallelization for a shared memory system.

The computer system used to generate results is a Dell Workstation with dual quad core Xeon X5355 processors running at 2.66 GHz with 16 GB of RAM. The operating system is Red Hat Enterprise Linux 5.2 Client.

2.2 Baseline Model Description

2.2.1 Drum and Overpack Geometry

As the problem is specifically concerned with the flux in waste drums, the first step is to identify the problem geometry. The waste stream under consideration is typically stored in either 55-gallon or 30-gallon drums. The SOW requires modeling of only one of these two sizes, since it is expected that that the findings will be relatively similar. The 55-galon size was selected to emphasize scattering effects.

The reference drum was a 55 gallon type based on the 1976 ANSI material handling specification for steel drums and pails. Based on this specification, the drum was represented in MCNP5 as accurately as possible.

The drum is a cylinder 87 cm tall with a 29 cm radius. The wall, top, and bottom thickness is 1.4 mm. The bands that circle the drum are stampings formed during the creation of the wall for ease in handling and strength. The drum is shown in Fig. 2.1. Fully detailed drawings are provided in the Appendix A.

Figure 2.1: Reference drum (black) with overpack (grey) cut away to expose the drum inside

2.2.2 Materials and Compositions

The waste matrix composition can vary greatly. It is an organic/combustible mixture of what would be found in the drum with operational waste such as latex gloves, paper towels, wood-based material, etc. The main isotopes it includes are C, H, O, F, and Cl. A range of combinations of individual fractions and densities are possible. The best estimate is given in Table 2.1. It is expected that using the exact composition for each individual drum (even if known) would not be necessary. However, to bound the impact of the uncertainty in the waste matrix composition assumption, additional simulations were performed that have 100% of each of those materials as a way to check what the effect is on the spectrum of each element.

Material	Weight Percent of Composition
Hydrogen	60 %
Carbon	30 %
Oxygen	10 %

Table 2.1: Waste matrix composition (best estimate)

For each variation of the materials inside the drum, there were four densities used: 0.1, 0.2, and 0.5 g/cm^3 with 0.2 g/cm^3 being the best estimate of what would be expected. These varying densities allowed a wide margin to see what the effects of the density change were on the spectra.

The drum and the overpack container were composed of the same material, 1018 steel. This is a mild grade steel with low carbon content. The drum in practice would normally be painted so it is not necessary to have the expense of a stainless steel. The elemental make up of the steel is given in Table 2.2.

Material	Weight Percent of Composition
Iron	98.81 %
Manganese	0.9 %
Carbon	0.2 %
Sulfur	0.05 %
Phosphorus	0.04%

Table 2.2: Composition of drum steel

The density of this material is 7.8 g/cm^3. Obviously, with this density and composition, the iron in the material dominates all the properties.

The final material in the simulation was air. It was necessary to model it even with its low density because part of the input required a non void streaming path. Its composition was based on the United States Standard Atmosphere of 1976 (USSA), as given in Table 2.3. The density of air in all locations was 0.001292 g/cm^3.

Material	Percent of Composition
Nitrogen	78.1 %
Oxygen	21.0 %
Argon	.934 %
Carbon (from CO_2 and CH_4)	0.0316 %
Neon	0.00182 %
Helium	0.000524 %
Xenon	0.0000087 %
Hydrogen (from H_2O and CH_4)	0.0000025 %

Table 2.3: Composition of air

2.2.3 Source

The reference source for this simulation was an isotropic point source in the middle of the drum emitting 0.662 MeV gammas corresponding to ^{137}Cs. The point source model helps eliminate some variability in the source, and the effect of multiple sources is simply their superposition. Most likely, a spatial source distribution is more realistic; however, depending on the distance of the detector from the drum and the waste matrix density, the effect will be minimized.

2.2.4 Overall Layout

The overall layout of the real system (Fig. 2.2) would have the drum on a rotating table with the detector(s) in a fixed position(s). As the drum is rotated, each detector would take a count of the gammas and that would be processed to quickly determine the possible sources and activity levels. In this model, the drum is by itself, as if suspended in air, as all elements of the room are not in the model. This was a simplification made in the baseline case to enable investigating scattered flux from drum and the material inside without interference with room/wall effects. It is also necessary to make this assumption because there is no information about the room that this apparatus would be housed in. However, perturbation cases will include the floor to evaluate its effects.

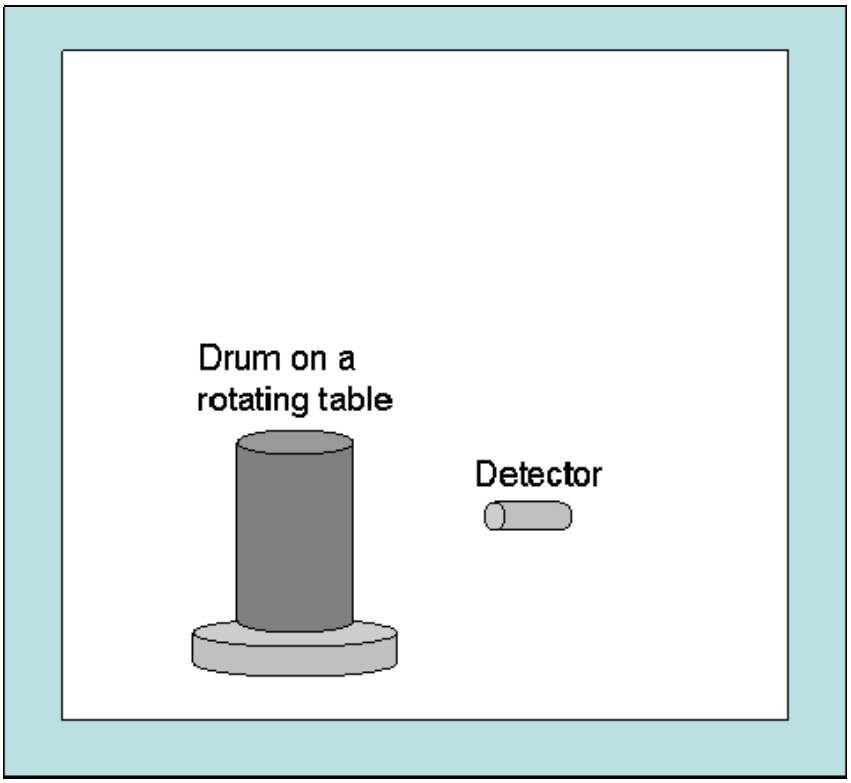

Figure 2.2: Actual layout schematic

2.2.5 The Reference (Baseline) Case

The baseline case consisted of these variables:

- No overpack
- 0.662 MeV isotropic centrally located source
- Best estimate waste material composition at 0.2 g/cm^3
- Drum isolated in air without room/walls

2.3 MCNP Model and Input

2.3.1 Input file

The MCNP model is a straightforward representation of the geometry and materials described in Section 2.2. The complete input file for the baseline case is provided in Appendix B.

2.3.2 Tallies

Several photon tallies have been implemented to obtain gamma-ray spectra at different locations. The model includes five different tallies at three locations and from two types: surface flux and ring detector. Note that the term "detector" does not imply any actual detector being modeled, but is merely the MCNP term for denoting a special type of tally.

The ring detector tally is a special type of tally based on the concept of a point detector tally. The point detector tally uses the next-event estimator to determine analytically contributions of particles to a certain location, at each collision, rather than only through tracking the particle history. Pseudoparticles with very low weights are calculated for every source particle and interaction. This psuedoparticle reaches the detector but its weight insures that the overall estimate will be valid. The ring detector is used when the problem has axial symmetry.

The ring detectors were placed in three locations: 50 cm from the source on plane, 130 cm from the source on plane, and 50 cm from the source and 25 cm below, as shown in Fig. 2.3.

The first ring detector is the most realistic location. It is expected that the detectors will be reasonably close to get the largest number of counts in the shortest amount of time. The other detector on plane can be used as a comparison to the closer one to possibly enable more accurate unfolding of the non-uniform source distribution from the difference between the two spectra acquired by the two detectors. The low ring detector is used as a way to minimize the source configurations necessary. A detector placed off plane will read the flux that is angled away from the on plane detectors giving an idea to what a stack of detectors might be able to count, or (through interpolation/superposition)

what the effect of a line source may be. The ring detectors greatly increased the efficiency of the simulation at the expense of small wall clock time increase.

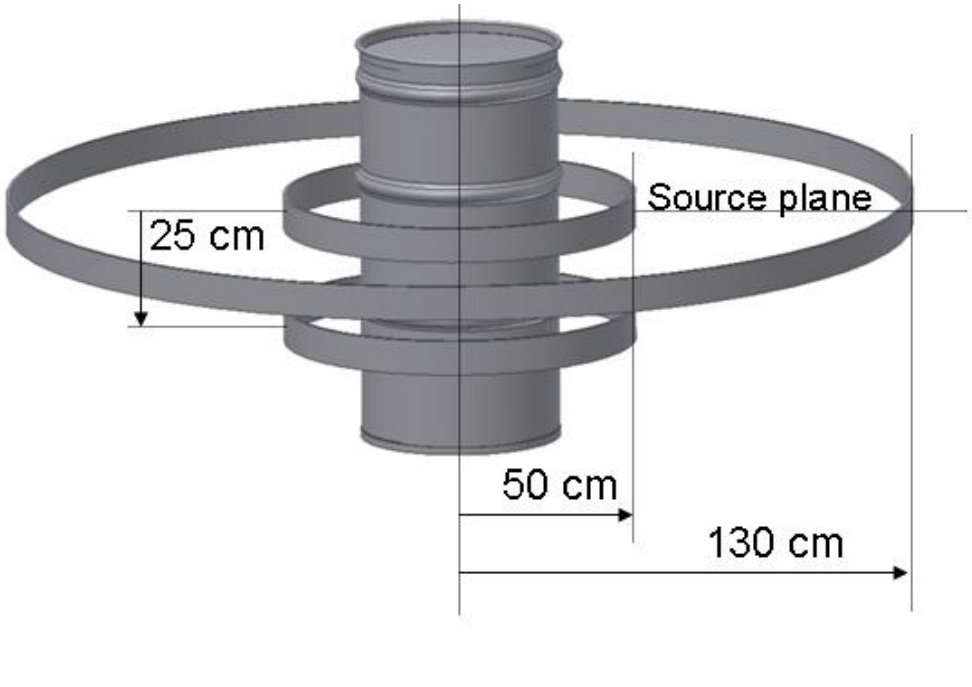

Figure 2.3: Tally locations

The two near detectors are 11 cm from the overpack when that option was added to the simulation. The location did not change between the two conditions when the overpack was present and when it was not.

The two surface flux tallies used were standard MCNP tallies of F2 type. They were used as a check for the ring detectors. The surface flux tallies were placed in the same location and the same size as the two ring detectors that are axially on the source plane.

2.4 Variation of the baseline model/case

2.4.1 Overpack

Within the confines of the problem definition, there are several variables that were to be specified or selected to develop the model. One of the specifically mentioned ones was the presence of the overpack container. The 9 cm of steel around the drum reduces the number of particles reaching the tallies, increasing scattering and worsening the statistics. This is one of the major variables because of the effect that it has on the discernable information that can be gathered from the simulation. Most of the simulations were therefore performed both with and without the overpack..

2.4.2 Waste Matrix Density

The baseline waste matrix density is 0.2 g/cm^3 with variations from 0.1 to 0.5 g/cm^3. This variation, along with the empty drum simulation, is designed to see if there are significant spectral differences between the different elements in the drum. The simulation results, in turn, could be used to unfold the contents and provide an approximate elemental makeup. It is expected that the densities will be low because of the nature of the material being stored.

2.4.3 Material Composition

There are five compositions of the waste matrix material used in the simulations: air, hydrogen only, carbon only, oxygen only, and the "best estimate" composition (Table 1). The main purpose of the variation is to compare the best mix with its individual constituents as well as see the effect of the drum on the spectra. Assuming that the whole matrix is composed of a single element is unrealistic, but it bounds the range of realistic variation. Air is taken to be the empty drum.

2.4.4 Source

The source has three variables: energy, shape/distribution, and position. The three considered energies originate from the two isotopes ^{137}Cs and ^{60}Co. ^{137}Cs is used in the baseline case with ^{60}Co for the perturbation. ^{60}Co was added because it is another likely source for activity after ^{137}Cs.

The shapes correspond to two different specifications of point source and line source. The point source is the baseline. The line source is modeled as either a line or a collection of points.

The final variation in the source is the location which is one of the reasons that there are multiple detector locations. As the position varies through the drum, there should be a corresponding azimuthal increase or decrease of flux when the detectors are binned in angle in the radial direction. The point source in the center of the drum located 50 cm from the bottom is used in the baseline case.

3. Analysis Performed and Results

3.1 Baseline Simulations and Presentation of Results

The standard assumptions for baseline simulation are:

- No room geometry
- No overpack
- ^{137}Cs isotropic point source
- Best estimate drum fill material, uniformly distributed
- 0.2 g/cm^3 fill density

The individual MCNP runs all simulated 200 million source photons and with the hardware, this equated to about 10^5 particles per second. This meant that in real time, runs took anywhere from 30 to 75 minutes depending on the density of the fill material.

For each simulation, there is a standard output. Each tally has 500 energy bins when the source is ^{137}Cs, equaling 1.33 keV per bin. When the source is ^{60}Co, there are 1000 bins ensuring that there is enough bins to cover the entire spectrum keeping the bin size the same for comparison. This fine structure was used because it is always possible to easily coarsen the bins (combining them) without having to run another simulation.

Results of all simulations are presented in consistent figures and tables that follow, one for each MCNP simulation. Each figure, as illustrated in Fig. 3.1 depicts gamma-ray spectra for the three ring detector tallies plotted with the energy on the abscissa and the normalized flux plotted logarithmically on the ordinate.

Below each figure there are two tables. The first table contains all the physical details about this particular simulation. From the list/table of runs, the individual record is pulled out for reference that includes all the necessary information.

The next table contains the information extracted from the spectrum that characterizes each case. It includes the uncollided and collided fluxes, with their statistical uncertainty, as well as their ratio.

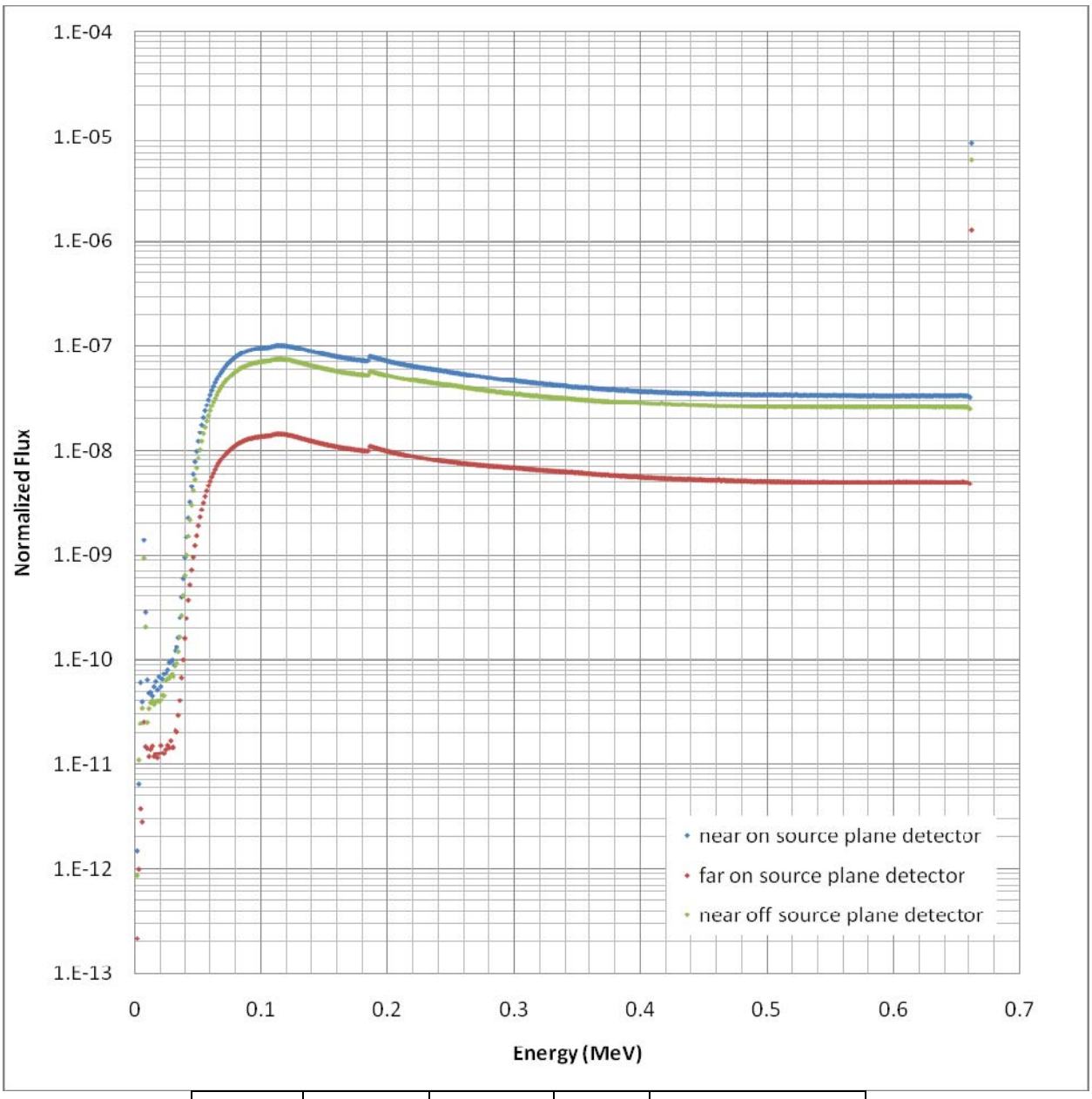

	Isotope	Material	Overpack	Source	Density (g/cm^3)
13	Cs-137	Best Est.	No	Point	0.5

	Collided Area	Sigma	Uncollided Area	Sigma	Ratio	Sigma
near on source plane	2.32E-05	3.60E-09	8.75E-06	2.62E-09	0.377	0.0001
far on source plane	3.32E-06	4.27E-10	1.28E-06	2.57E-10	0.386	0.0001
near off source plane	1.72E-05	3.19E-09	6.01E-06	1.80E-09	0.349	0.0001

Figure 3.1: Sample results

3.2 Effects of Main Assumptions and Approximations in Simulations

3.2.1 Using the Ring Detector Tally

One concern was about the accuracy of the ring detector. In all the simulations, there was a surface flux tally at the same location as the ring detector. The surface flux tally does not require the additional pseudoparticle calculation, and was included as a check to see if there were any issues with the ring tally. The surface tally has a larger statistical uncertainty, but still small enough to enable detecting anomalous behavior.

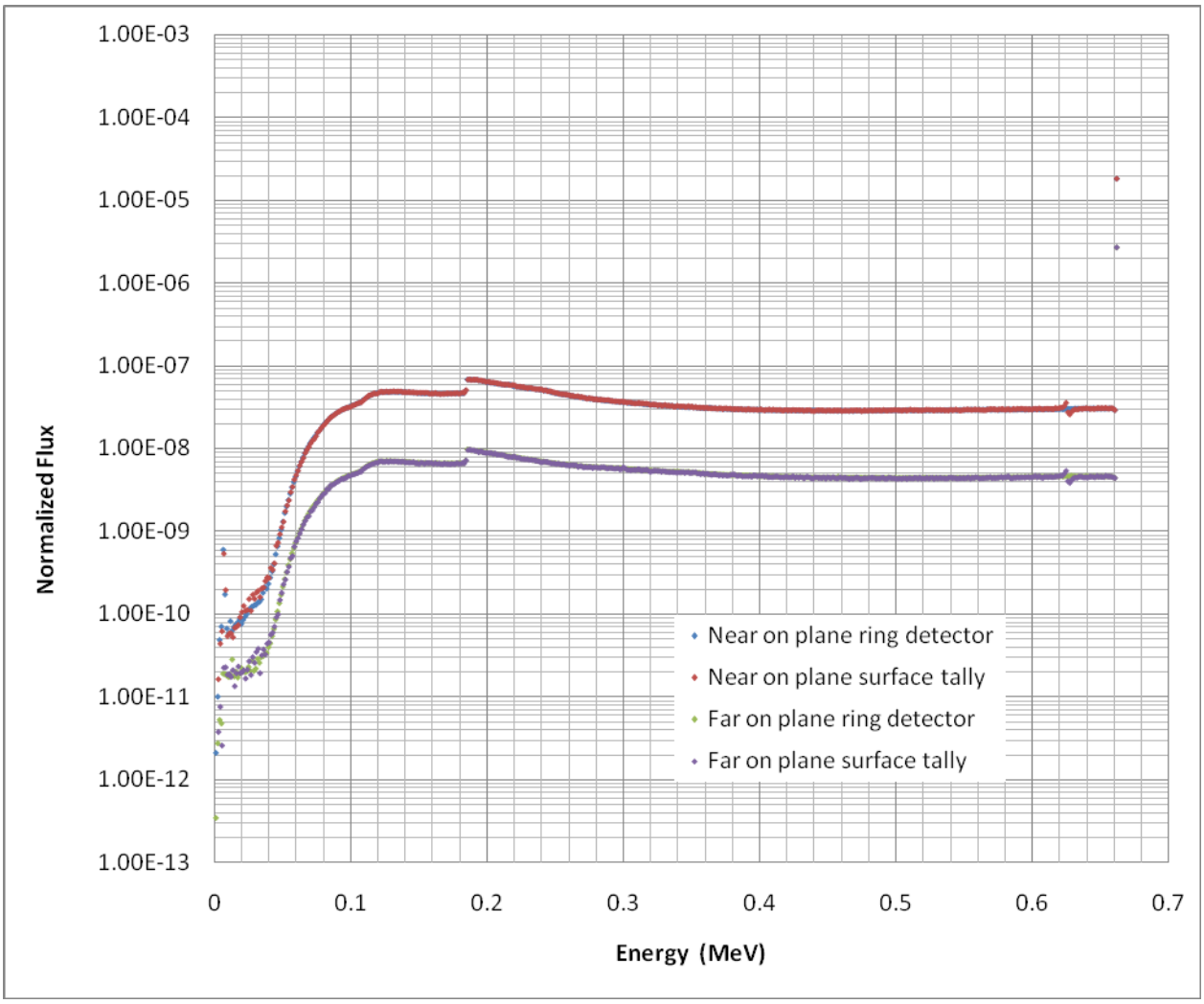

Figure 3.2: Surface tally and ring detector comparison

The spectra obtained by F2 surface tally and F5 detector tally, for the near and far detector, are shown in Figure 3.2. As it can be clearly seen from the figure, the corresponding spectra in each case overlap for all energies over 50 keV. Energies below 50 keV may be ignored because the statistics were poor for those bins due to scattering and ttenuation.

3.2.2 Number of particles vs statistics

Statistically, running 200 billion source particles resulted in excellent (low) sigmas that were on the order of one percent for individual energy bins above 100 keV. The low energy bins had significantly higher uncertainty, as expected, as there should not be that many low energy particles reaching the detector location.

3.2.2 Drum Fill Material Composition

One of the significant issues is the fill material in the drum. It is almost impossible to determine what the exact composition is. The assumption of the best estimate is a very broad one. Part of the analysis with the fills that are 100% of a single element is to determine if there is a way to unfold the contents knowing the spectra of the constituents.

3.2.4 Room and Wall Effects

The location where the drum will be placed is a concern, which is what early iterations of this model concluded. The impact of the floor and walls can cause additional scatterings to be recorded changing the results. Since there was no information about the room where the detection will take place, it was left out to minimize the variables, but may be addressed in future studies.

3.3 Cases Analyzed

The matrix of various cases analyzed is given in Table 3.1. Each run is identified by a Run ID, followed by values of other parameters. There are 29 cases, and results (spectra and peak-to-total Compton ratio) for these cases follow in Fig. 3.3 to 3.33. In the case of cobalt source, with two characteristic source energies, the table with results has been modified accordingly.

3.4 Analysis of Results

3.4.1 Some general/systematic observations

All the results (spectra) have been shown on the identical logarithmic scale for easy comparison. In general, with the increase in density, there is an increase in the amount of scattered flux, in particular in the lower energy range, due to multiple scattering. Specific comparisons and analysis are in the following sections.

	Isotope	Material	Overpack	Source	Density (g/cm^3)
1	Cs-137	Empty	No	Point	0.001292
2	Cs-137	Hydrogen	No	Point	0.1
3	Cs-137	Hydrogen	No	Point	0.2
4	Cs-137	Hydrogen	No	Point	0.5
5	Cs-137	Carbon	No	Point	0.1
6	Cs-137	Carbon	No	Point	0.2
7	Cs-137	Carbon	No	Point	0.5
8	Cs-137	Oxygen	No	Point	0.1
9	Cs-137	Oxygen	No	Point	0.2
10	Cs-137	Oxygen	No	Point	0.5
11	Cs-137	Best Est.	No	Point	0.1
12	Cs-137	Best Est.	No	Point	0.2
13	Cs-137	Best Est.	No	Point	0.5
14	Cs-137	Empty	Yes	Point	0.001292
15	Cs-137	Hydrogen	Yes	Point	0.1
16	Cs-137	Hydrogen	Yes	Point	0.2
17	Cs-137	Hydrogen	Yes	Point	0.5
18	Cs-137	Carbon	Yes	Point	0.1
19	Cs-137	Carbon	Yes	Point	0.2
20	Cs-137	Carbon	Yes	Point	0.5
21	Cs-137	Oxygen	Yes	Point	0.1
22	Cs-137	Oxygen	Yes	Point	0.2
23	Cs-137	Oxygen	Yes	Point	0.5
24	Cs-137	Best Est.	Yes	Point	0.1
25	Cs-137	Best Est.	Yes	Point	0.2
26	Cs-137	Best Est.	Yes	Point	0.5
27	Co-60	Best Est.	No	Point	0.2
28	Cs-137	Best Est.	No	Offset Point	0.2
29	Co-60	Best Est.	No	Point	0.5

Table 3.1: Composition of air

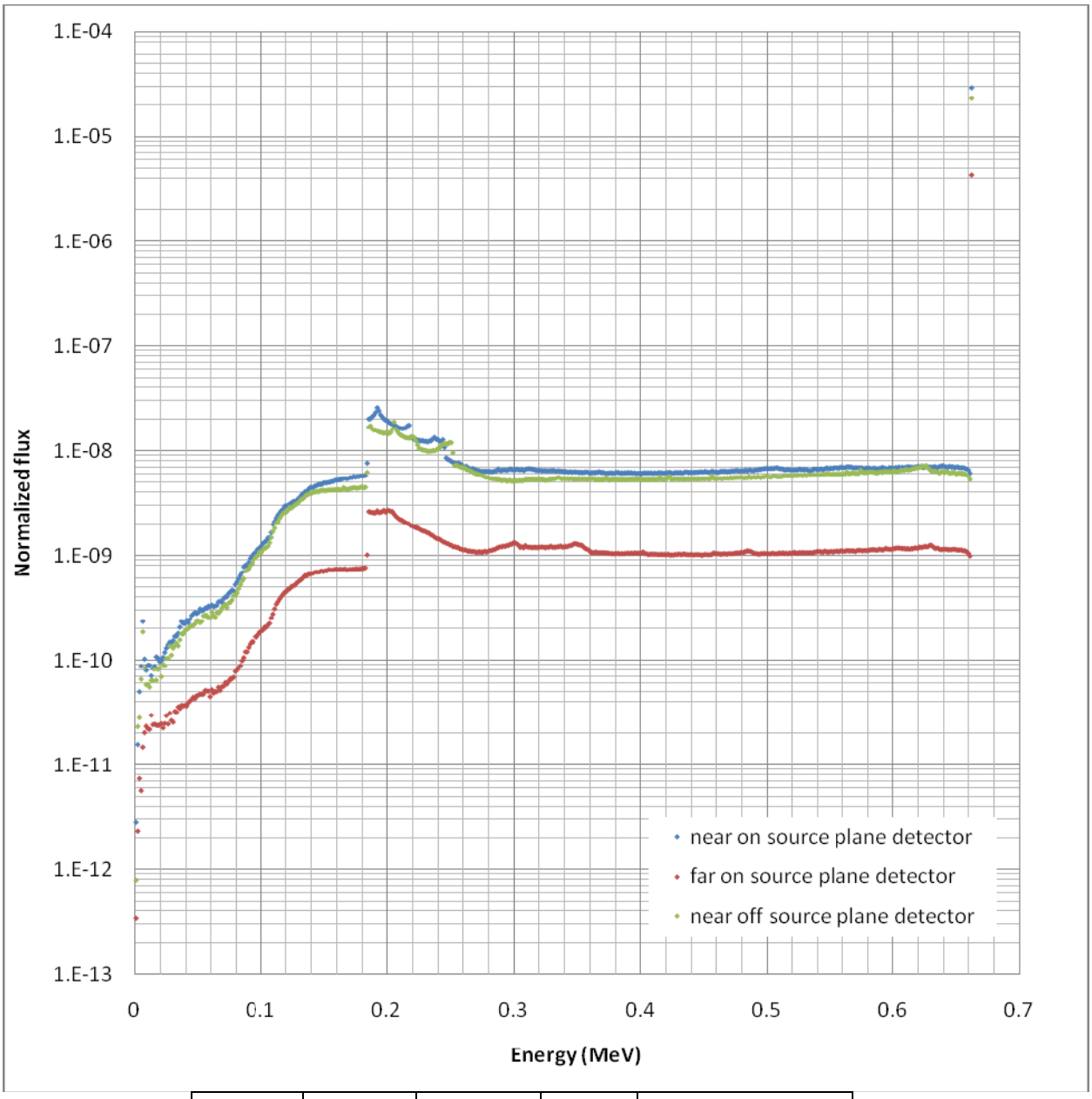

	Isotope	Material	Overpack	Source	Density (g/cm^3)
1	Cs-137	AIr	No	Point	0.001292

	Collided Area	Sigma	Uncollided Area	Sigma	Ratio	Sigma
near on source plane	3.24E-05	1.22E-09	2.93E-05	2.93E-09	0.904	0.0001
far on source plane	4.78E-06	1.73E-10	4.30E-06	4.30E-10	0.898	0.0001
near off source plane	2.59E-05	1.45E-09	2.32E-05	2.32E-09	0.896	0.0001

Figure 3.3: Results for run 1

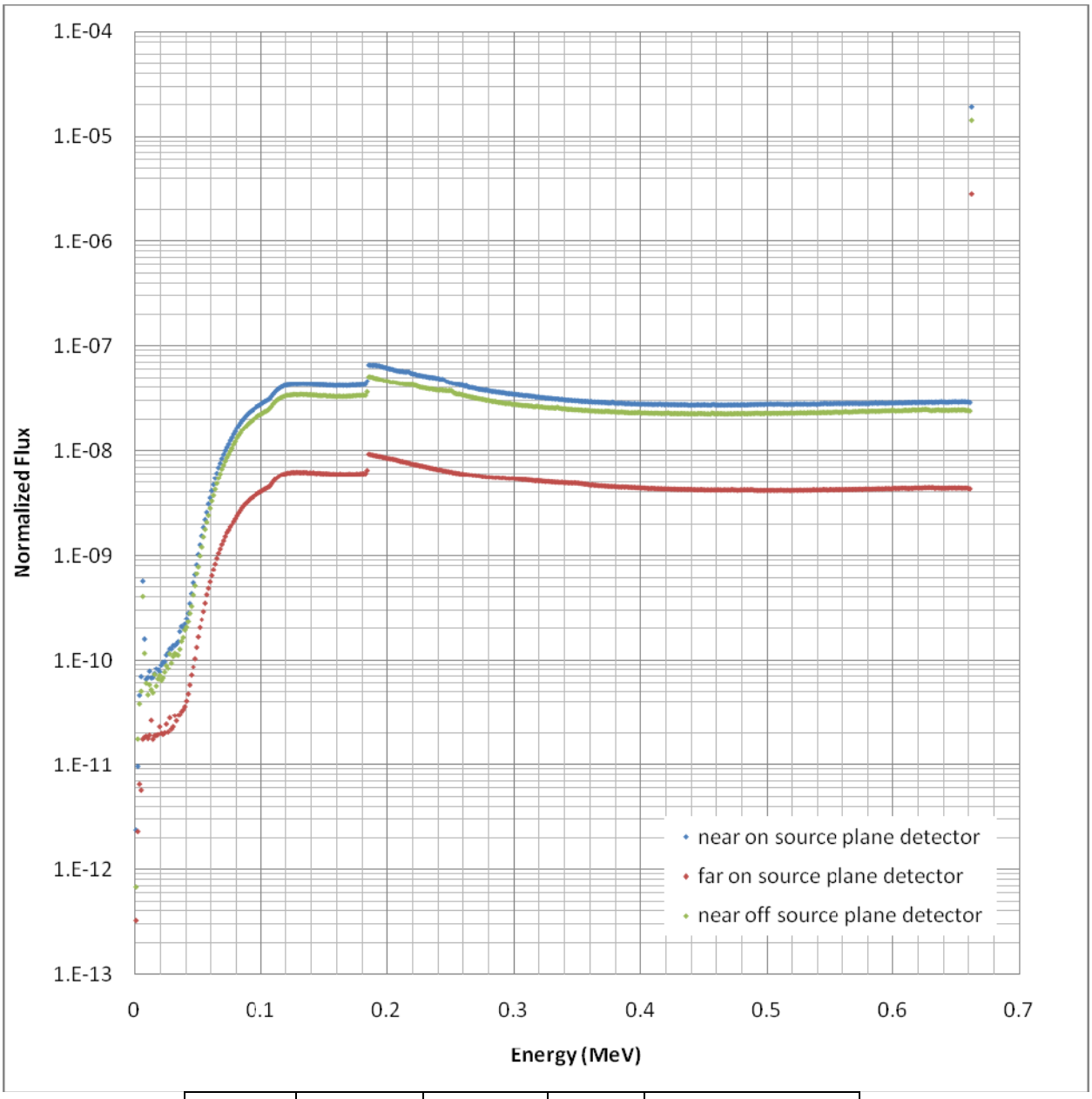

	Isotope	Material	Overpack	Source	Density (g/cm^3)
2	Cs-137	Hydrogen	No	Point	0.1

	Collided Area	Sigma	Uncollided Area	Sigma	Ratio	Sigma
near on source plane	1.51E-05	2.50E-09	1.90E-05	1.90E-09	1.26	0.0002
far on source plane	2.23E-06	3.16E-10	2.79E-06	2.79E-10	1.25	0.0002
near off source plane	1.23E-05	2.39E-09	1.43E-05	2.86E-09	1.17	0.0003

Figure 3.4: Results for run 2

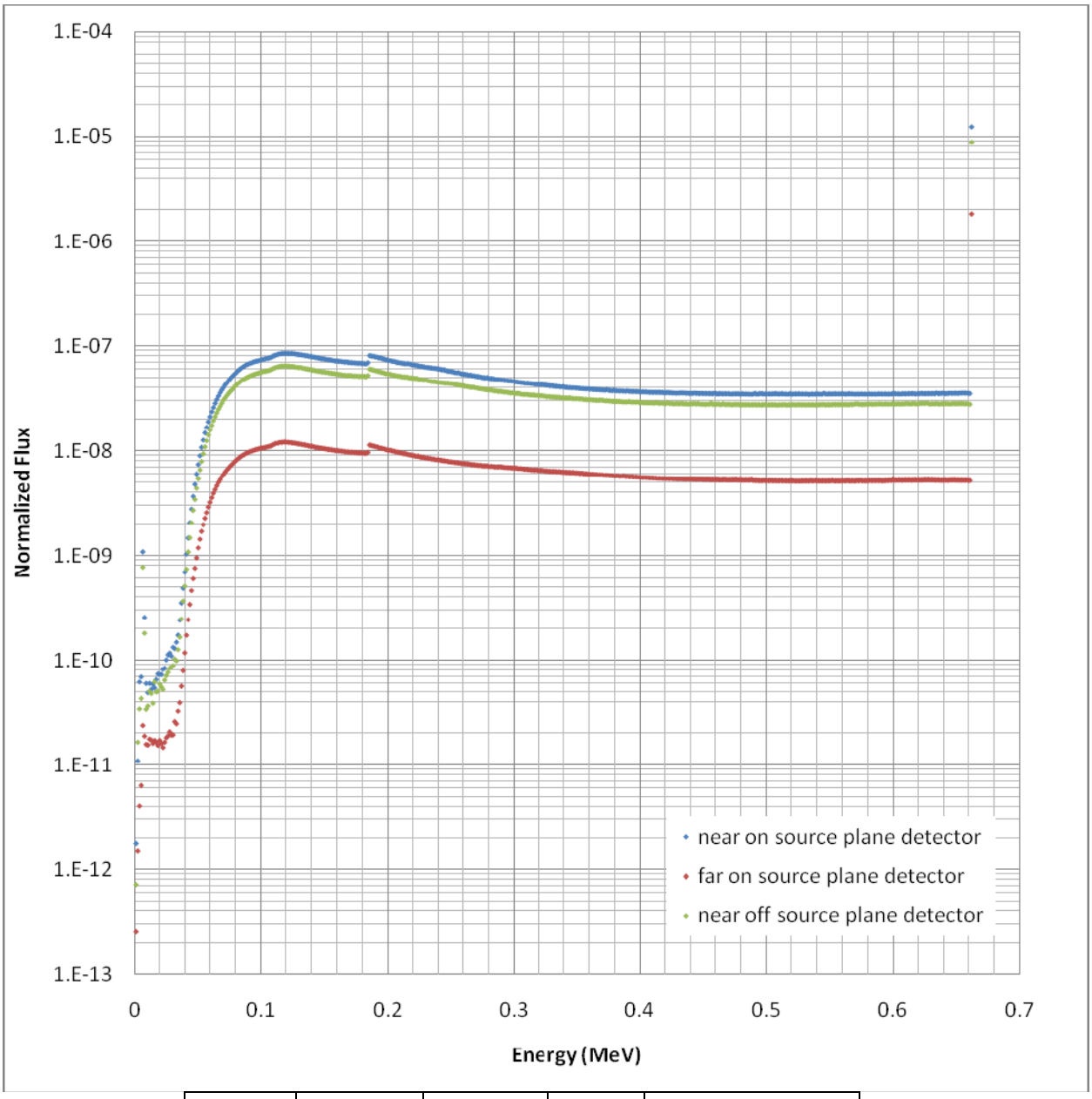

	Isotope	Material	Overpack	Source	Density (g/cm^3)
3	Cs-137	Hydrogen	No	Point	0.2

	Collided Area	Sigma	Uncollided Area	Sigma	Ratio	Sigma
near on source plane	2.16E-05	3.04E-09	1.23E-05	2.46E-09	0.568	0.0001
far on source plane	3.14E-06	3.83E-10	1.80E-06	1.80E-10	0.573	0.0001
near off source plane	1.67E-05	2.85E-09	8.78E-06	1.76E-09	0.526	0.0001

Figure 3.5: Results for run 3

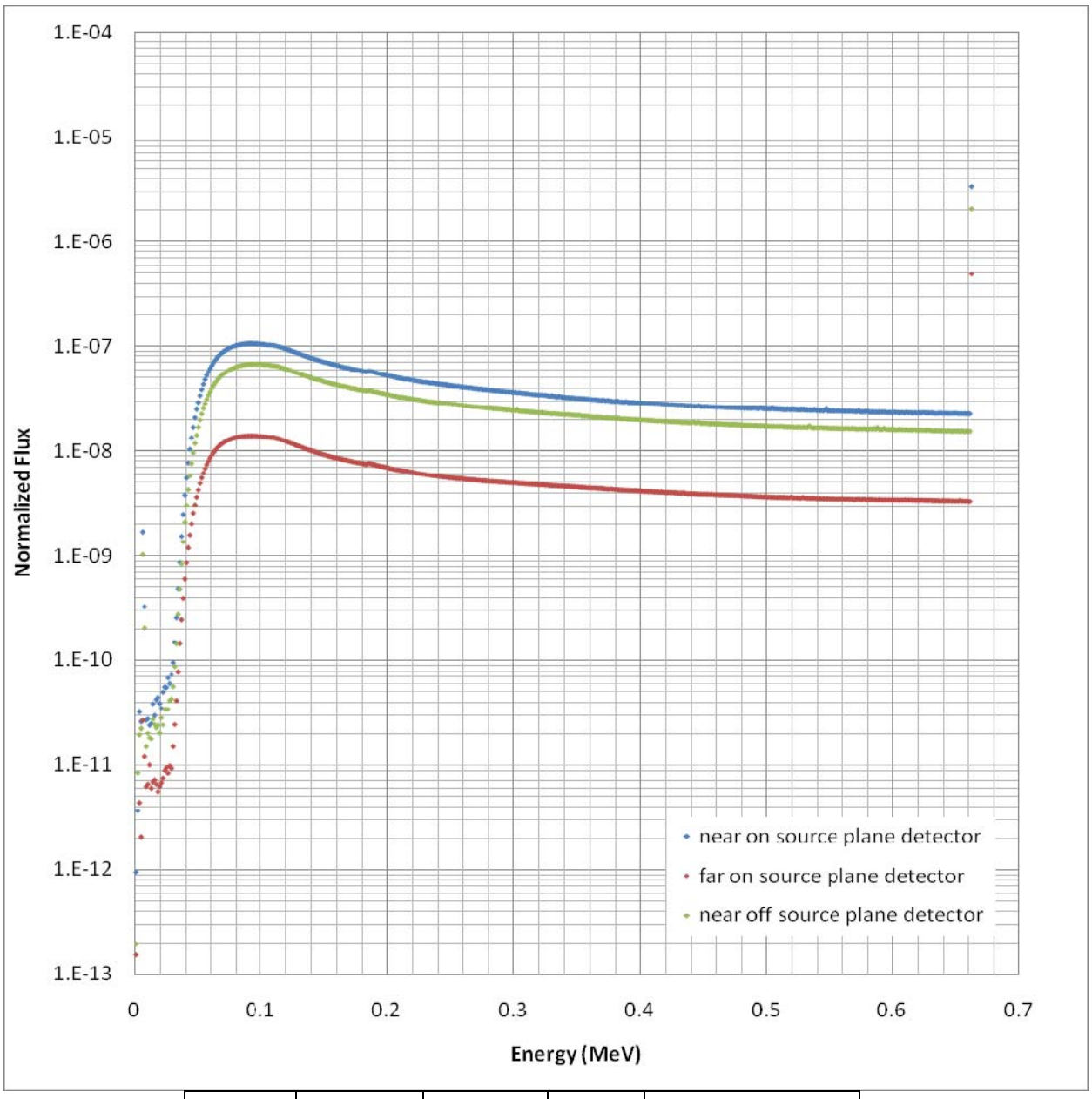

	Isotope	Material	Overpack	Source	Density (g/cm^3)
4	Cs-137	Hydrogen	No	Point	0.5

	Collided Area	Sigma	Uncollided Area	Sigma	Ratio	Sigma
near on source plane	1.94E-05	3.14E-09	3.32E-06	1.33E-09	0.171	0.0001
far on source plane	2.67E-06	3.23E-10	4.87E-07	9.74E-11	0.183	0.0000
near off source plane	1.29E-05	2.53E-09	2.04E-06	1.22E-09	0.158	0.0001

Figure 3.6: Results for run 4

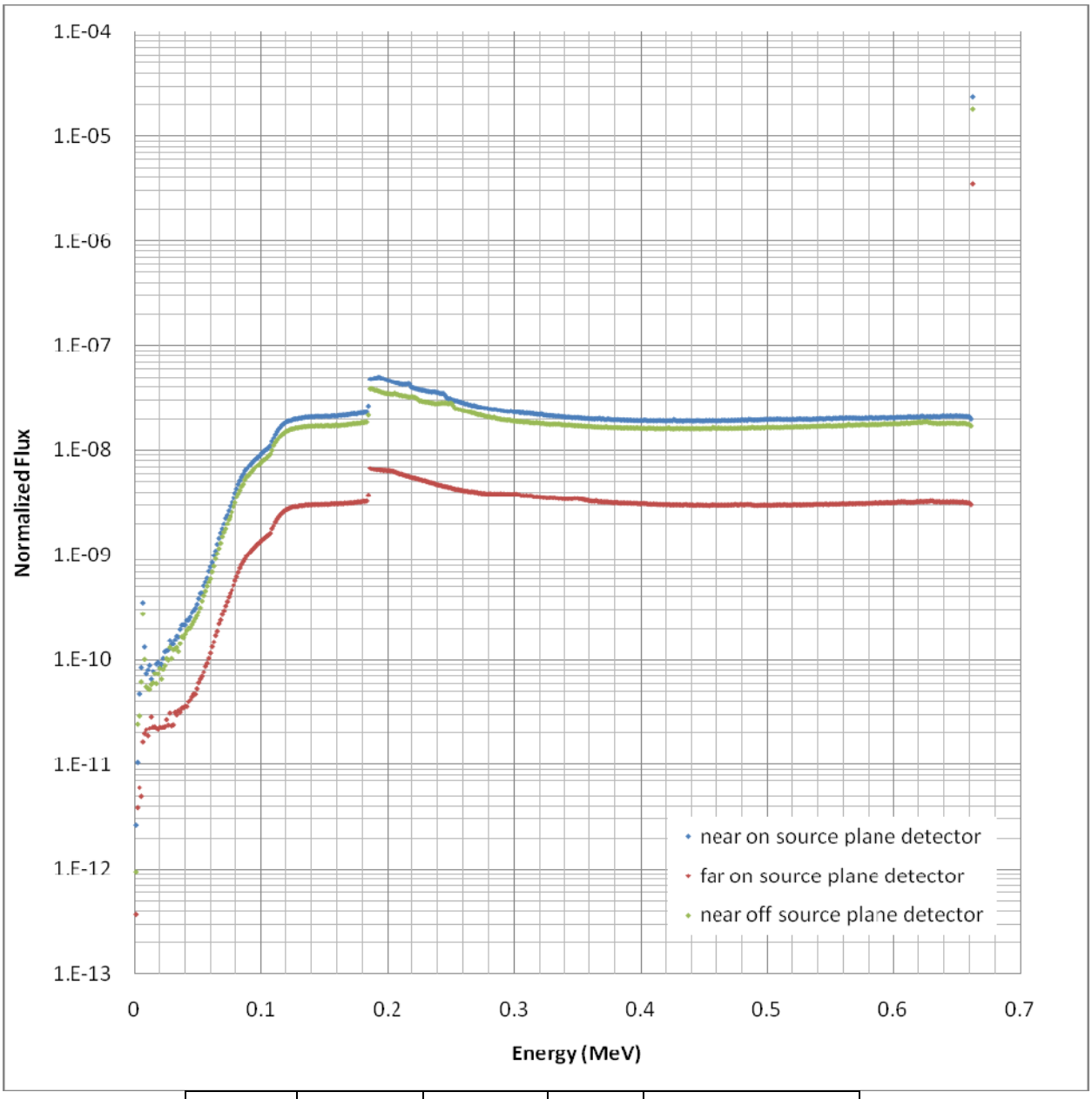

	Isotope	Material	Overpack	Source	Density (g/cm^3)
5	Cs-137	Carbon	No	Point	0.1

	Collided Area	Sigma	Uncollided Area	Sigma	Ratio	Sigma
near on source plane	9.81E-06	2.23E-09	2.36E-05	2.36E-09	2.403	0.0006
far on source plane	1.47E-06	2.83E-10	3.46E-06	3.46E-10	2.354	0.0005
near off source plane	8.17E-06	1.99E-09	1.82E-05	3.64E-09	2.229	0.0007

Figure 3.7: Results for run 5

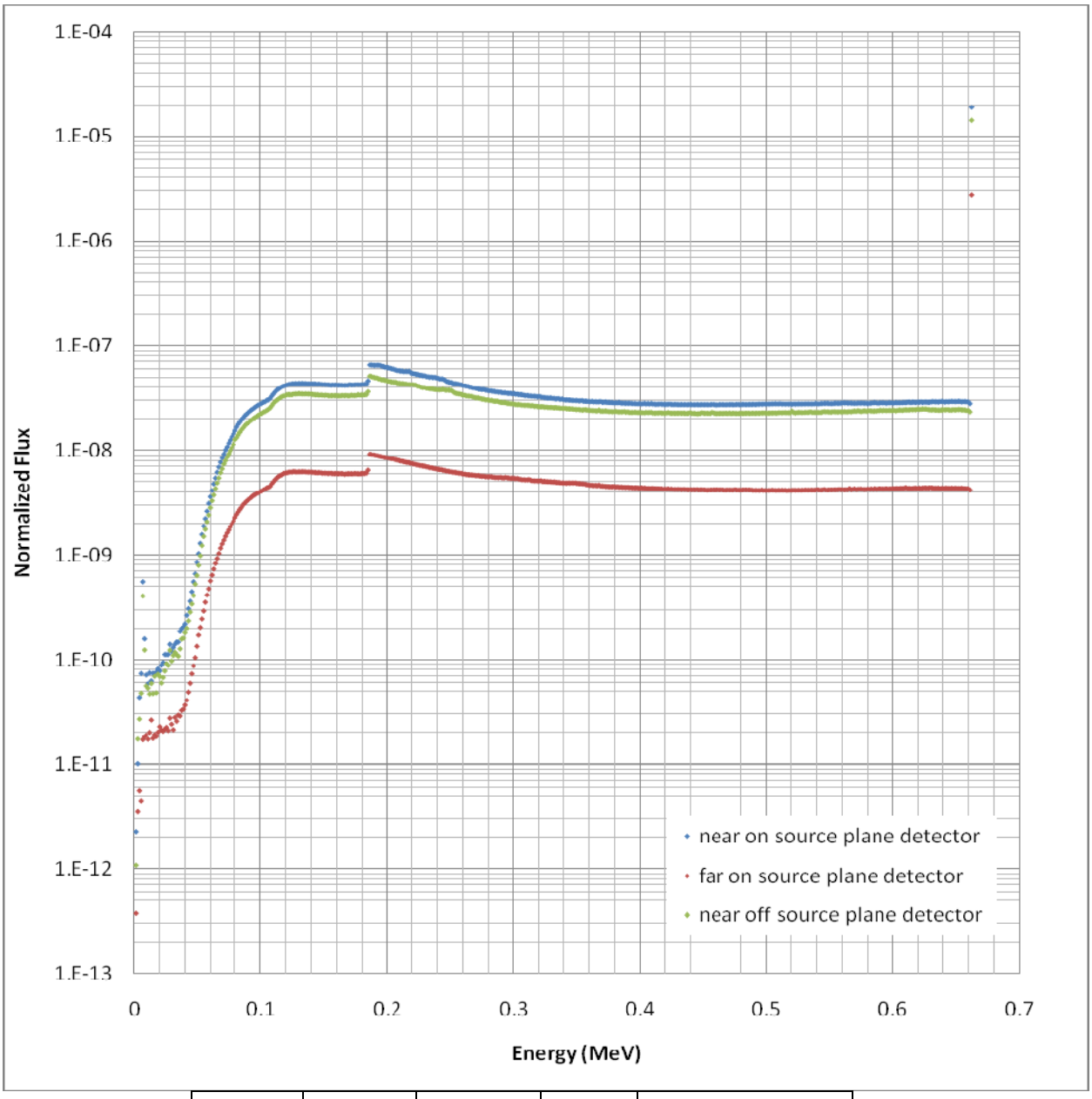

	Isotope	Material	Overpack	Source	Density (g/cm^3)
6	Cs-137	Carbon	No	Point	0.2

	Collided Area	Sigma	Uncollided Area	Sigma	Ratio	Sigma
near on source plane	1.51E-05	2.71E-09	1.89E-05	3.78E-09	1.250	0.0003
far on source plane	2.24E-06	3.70E-10	2.78E-06	2.78E-10	1.238	0.0002
near off source plane	1.23E-05	2.69E-09	1.42E-05	2.85E-09	1.157	0.0003

Figure 3.8: Results for run 6

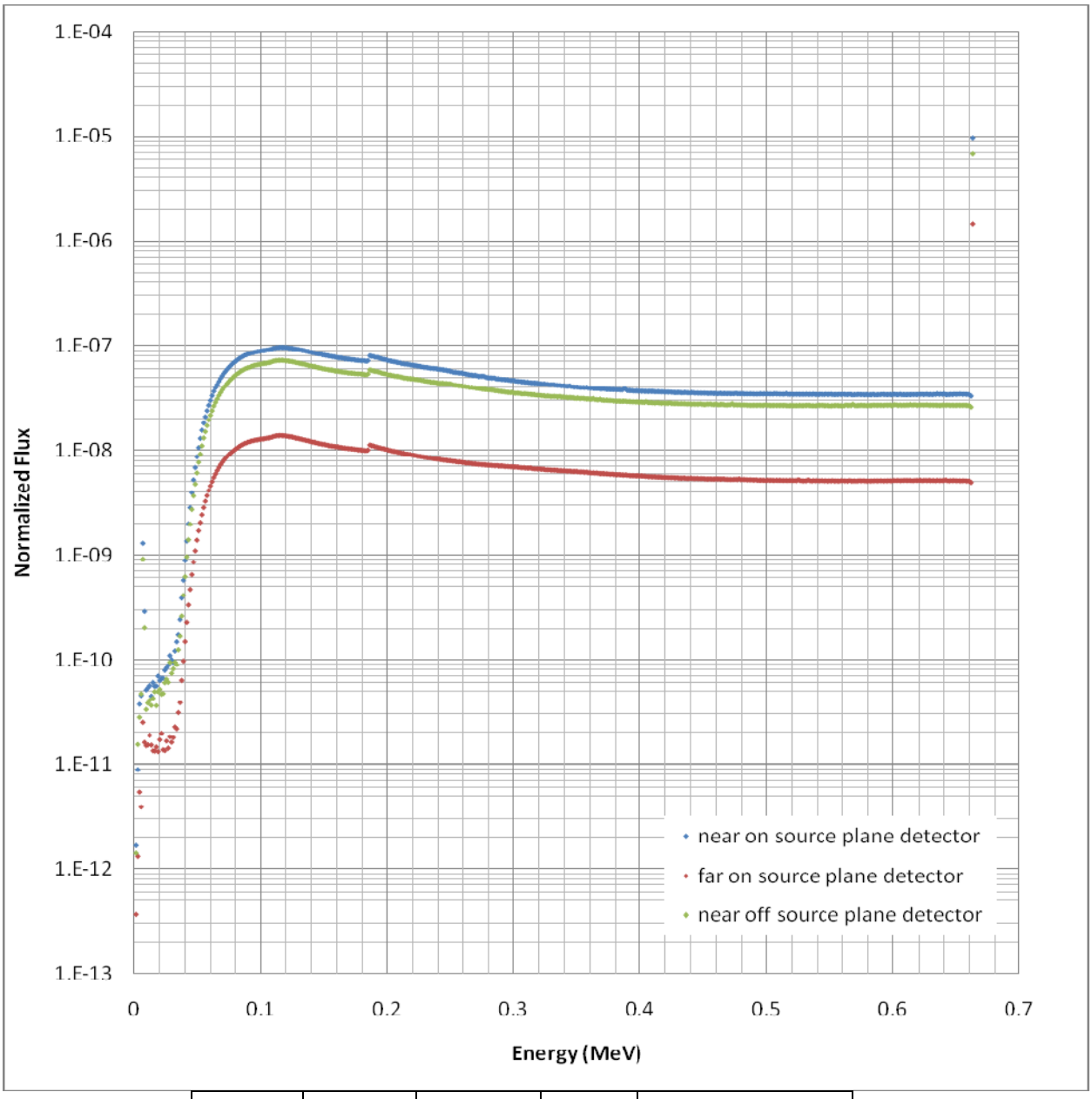

	Isotope	Material	Overpack	Source	Density (g/cm^3)
7	Cs-137	Carbon	No	Point	0.5

	Collided Area	Sigma	Uncollided Area	Sigma	Ratio	Sigma
near on source plane	2.29E-05	3.71E-09	9.79E-06	2.94E-09	0.427	0.0001
far on source plane	3.30E-06	4.42E-10	1.44E-06	2.87E-10	0.435	0.0001
near off source plane	1.73E-05	3.24E-09	6.82E-06	2.05E-09	0.395	0.0001

Figure 3.9: Results for run 7

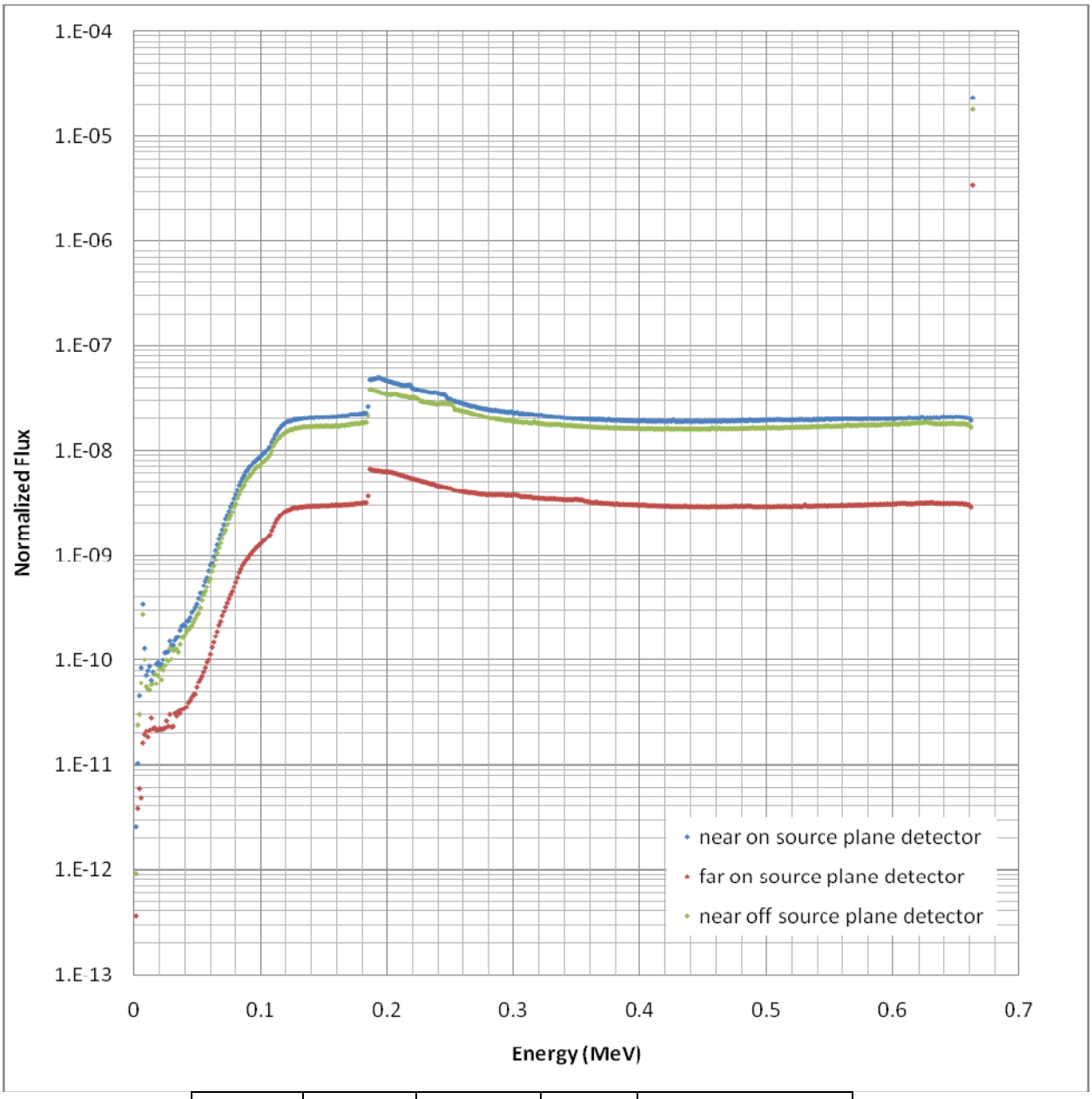

	Isotope	Material	Overpack	Source	Density (g/cm^3)
8	Cs-137	Oxygen	No	Point	0.1

	Collided Area	Sigma	Uncollided Area	Sigma	Ratio	Sigma
near on source plane	9.81E-06	2.28E-09	2.36E-05	2.36E-09	2.402	0.0006
far on source plane	1.47E-06	3.08E-10	3.46E-06	3.46E-10	2.353	0.0005
near off source plane	8.17E-06	2.17E-09	1.82E-05	3.64E-09	2.227	0.0007

Figure 3.10: Results for run 8

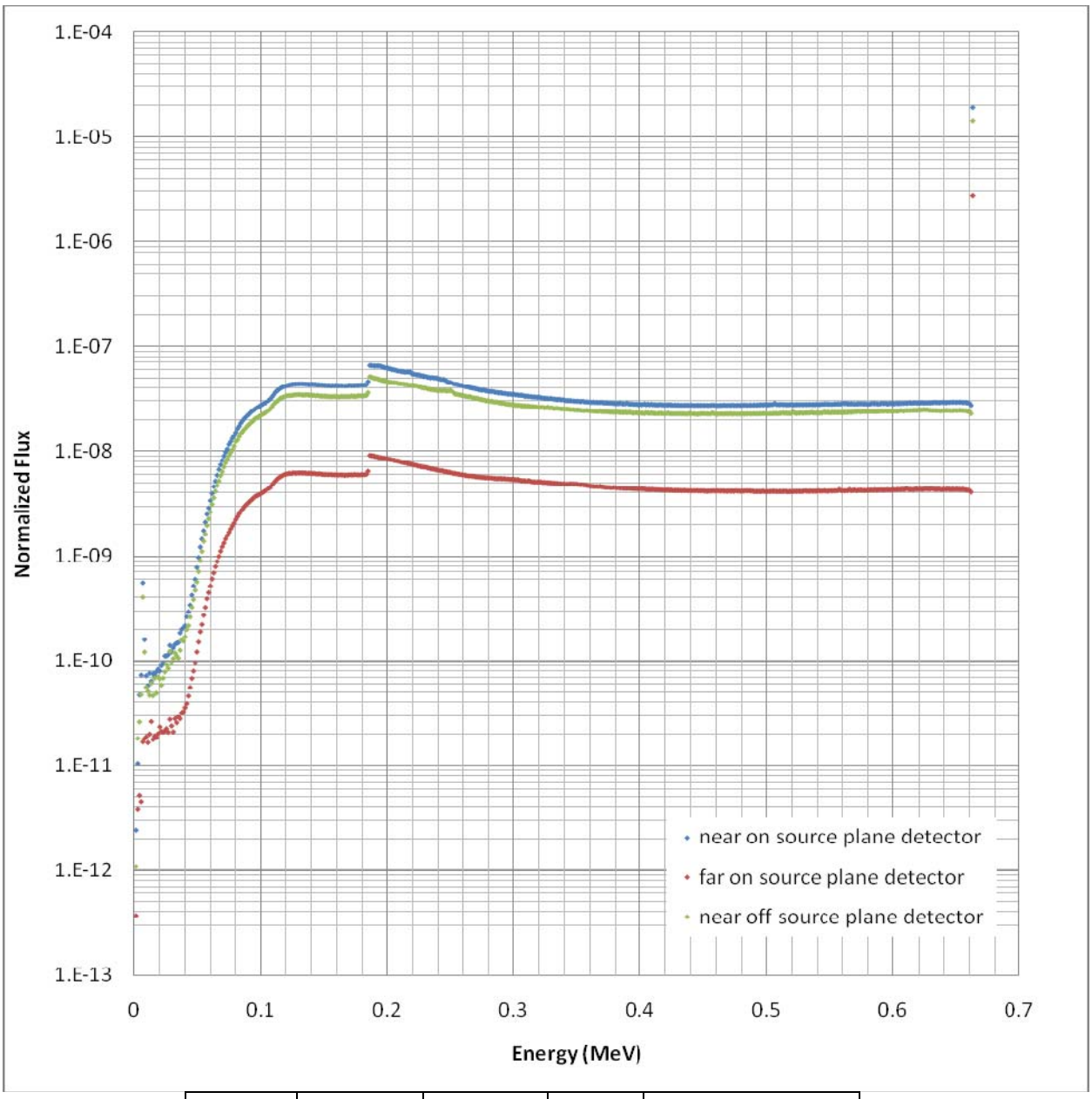

	Isotope	Material	Overpack	Source	Density (g/cm^3)
9	Cs-137	Oxygen	No	Point	0.2

	Collided Area	Sigma	Uncollided Area	Sigma	Ratio	Sigma
near on source plane	1.51E-05	2.97E-09	1.89E-05	3.78E-09	1.250	0.0004
far on source plane	2.24E-06	3.95E-10	2.78E-06	2.78E-10	1.239	0.0003
near off source plane	1.23E-05	2.88E-09	1.42E-05	4.27E-09	1.158	0.0004

Figure 3.11: Results for run 9

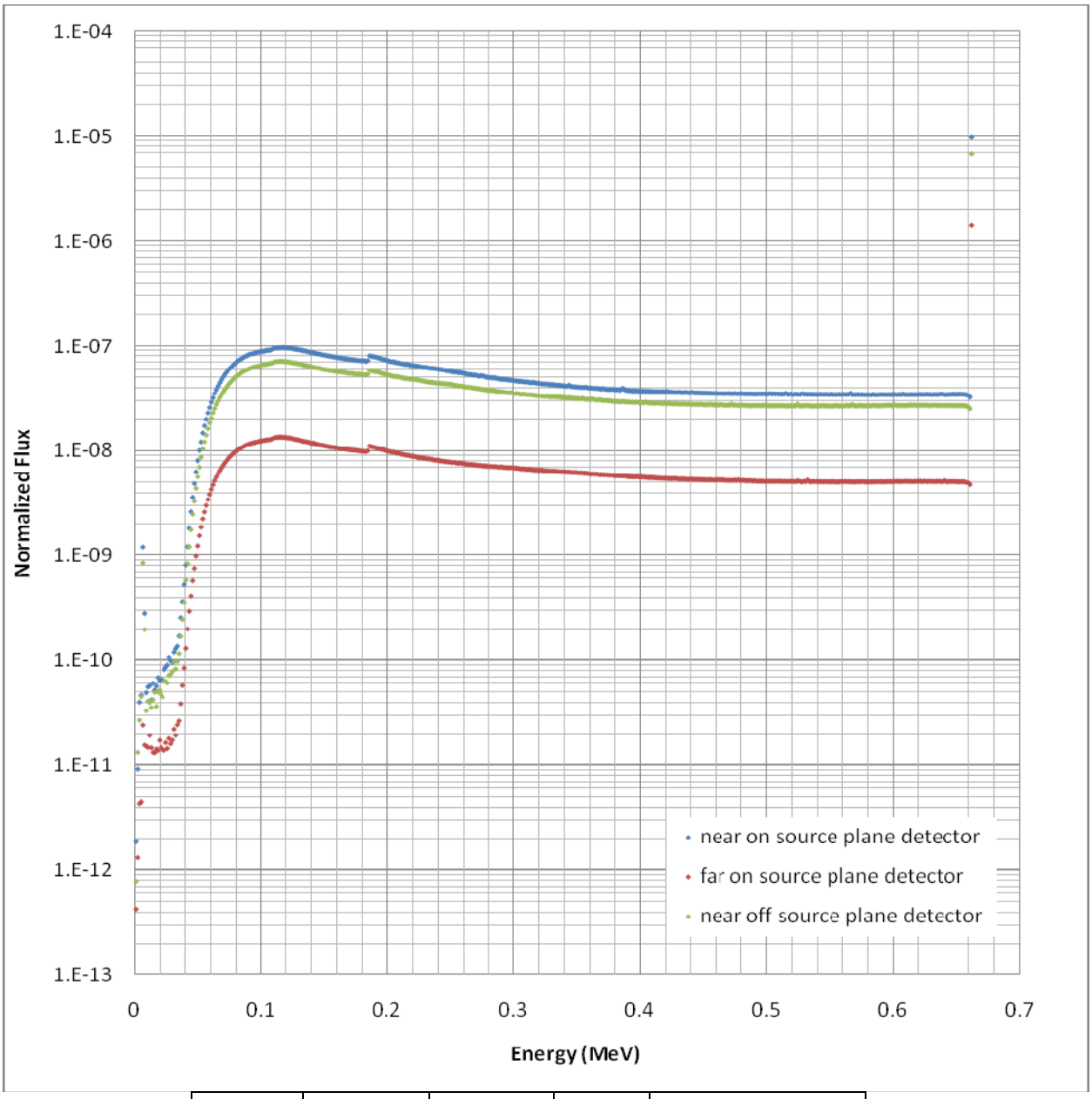

	Isotope	Material	Overpack	Source	Density (g/cm^3)
10	Cs-137	Oxygen	No	Point	0.5

	Collided Area	Sigma	Uncollided Area	Sigma	Ratio	Sigma
near on source plane	2.27E-05	4.10E-09	9.78E-06	2.93E-09	0.431	0.0002
far on source plane	3.27E-06	4.95E-10	1.44E-06	2.87E-10	0.439	0.0001
near off source plane	1.71E-05	3.53E-09	6.81E-06	2.04E-09	0.398	0.0001

Figure 3.12: Results for run 10

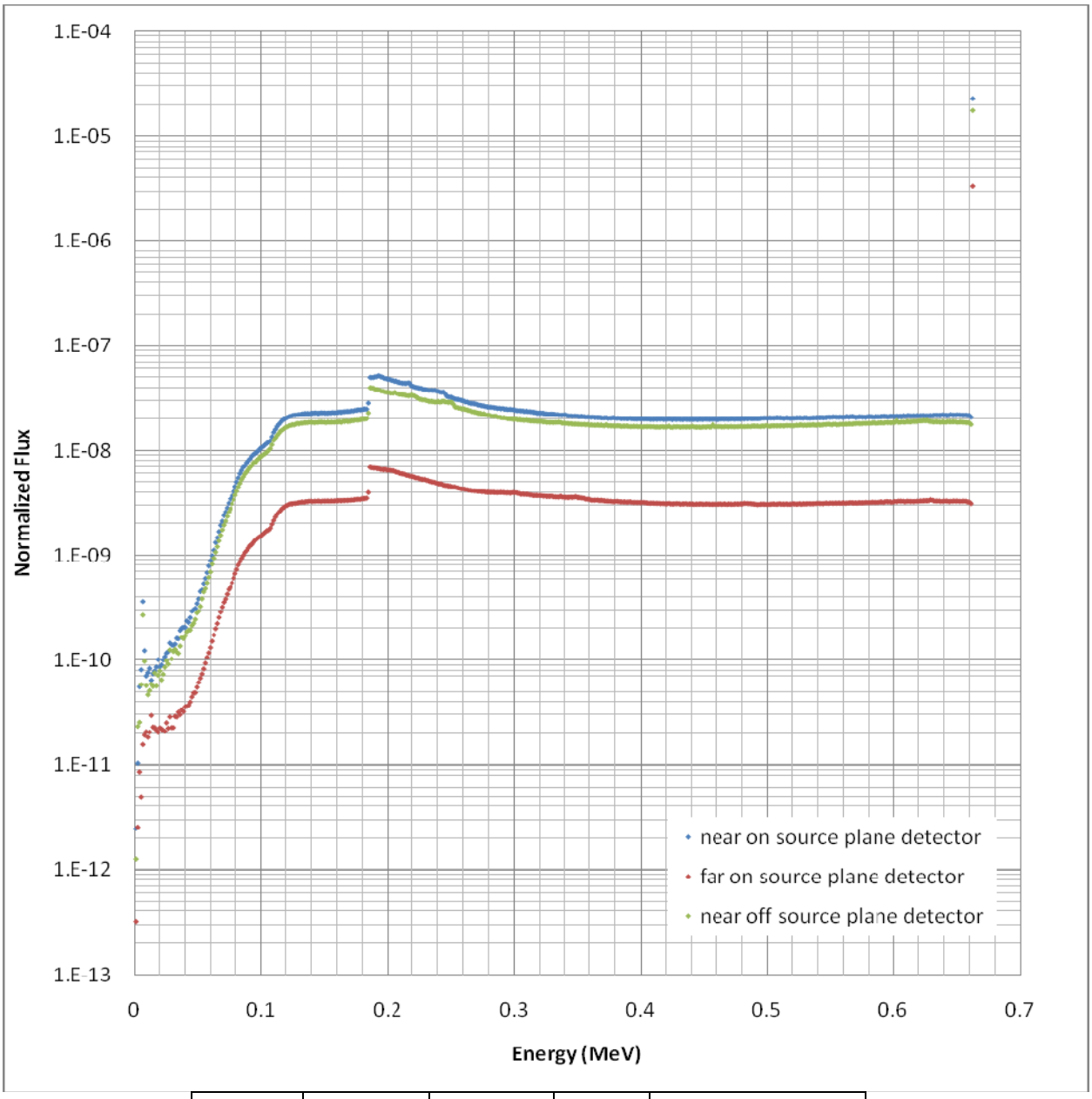

	Isotope	Material	Overpack	Source	Density (g/cm^3)
11	Cs-137	Best Est.	No	Point	0.1

	Collided Area	Sigma	Uncollided Area	Sigma	Ratio	Sigma
near on source plane	1.04E-05	2.29E-09	2.30E-05	2.30E-09	2.211	0.0005
far on source plane	1.56E-06	2.81E-10	3.38E-06	3.38E-10	2.169	0.0004
near off source plane	8.66E-06	2.19E-09	1.77E-05	1.77E-09	2.049	0.0006

Figure 31.3: Results for run 11

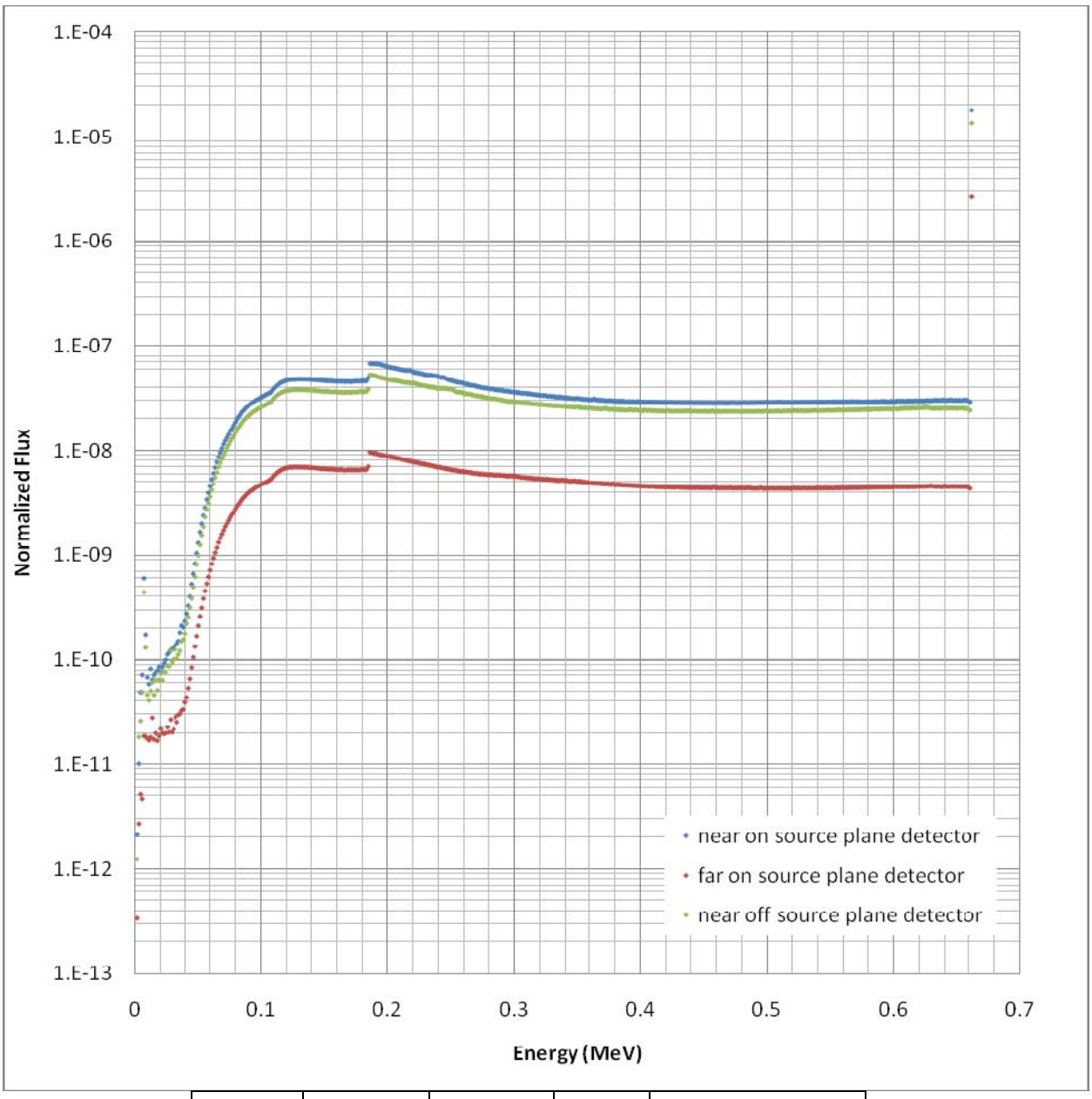

	Isotope	Material	Overpack	Source	Density (g/cm^3)
12	Cs-137	Best Est.	No	Point	0.2

	Collided Area	Sigma	Uncollided Area	Sigma	Ratio	Sigma
near on source plane	1.61E-05	2.85E-09	1.81E-05	3.62E-09	1.127	0.0003
far on source plane	2.37E-06	3.79E-10	2.65E-06	2.65E-10	1.118	0.0002
near off source plane	1.30E-05	2.66E-09	1.35E-05	2.71E-09	1.043	0.0003

Figure 3.14: Results for run 12

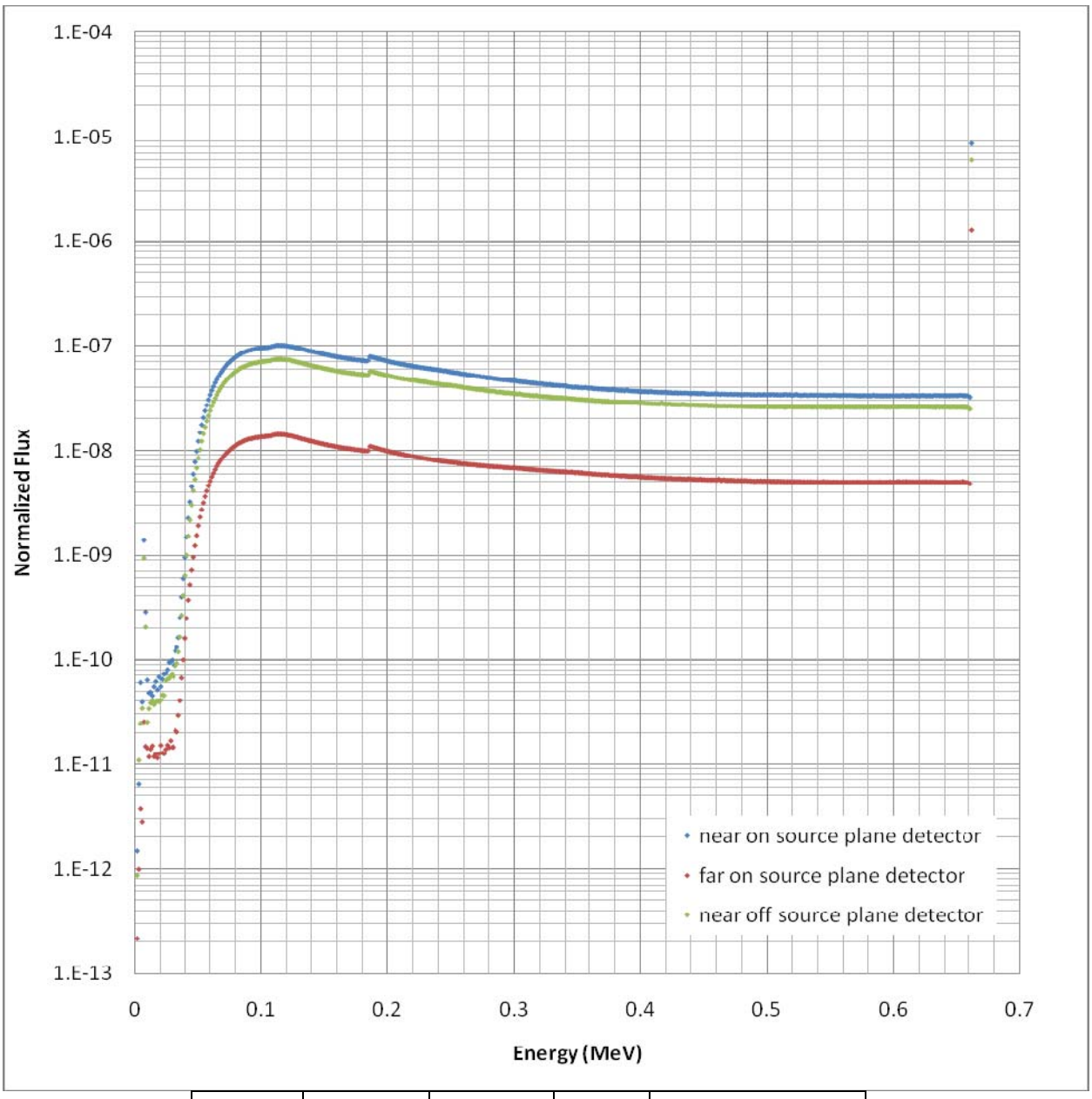

	Isotope	Material	Overpack	Source	Density (g/cm^3)
13	Cs-137	Best Est.	No	Point	0.5

	Collided Area	Sigma	Uncollided Area	Sigma	Ratio	Sigma
near on source plane	2.32E-05	3.60E-09	8.75E-06	2.62E-09	0.377	0.0001
far on source plane	3.32E-06	4.27E-10	1.28E-06	2.57E-10	0.386	0.0001
near off source plane	1.72E-05	3.19E-09	6.01E-06	1.80E-09	0.349	0.0001

Figure 3.15: Results for run 13

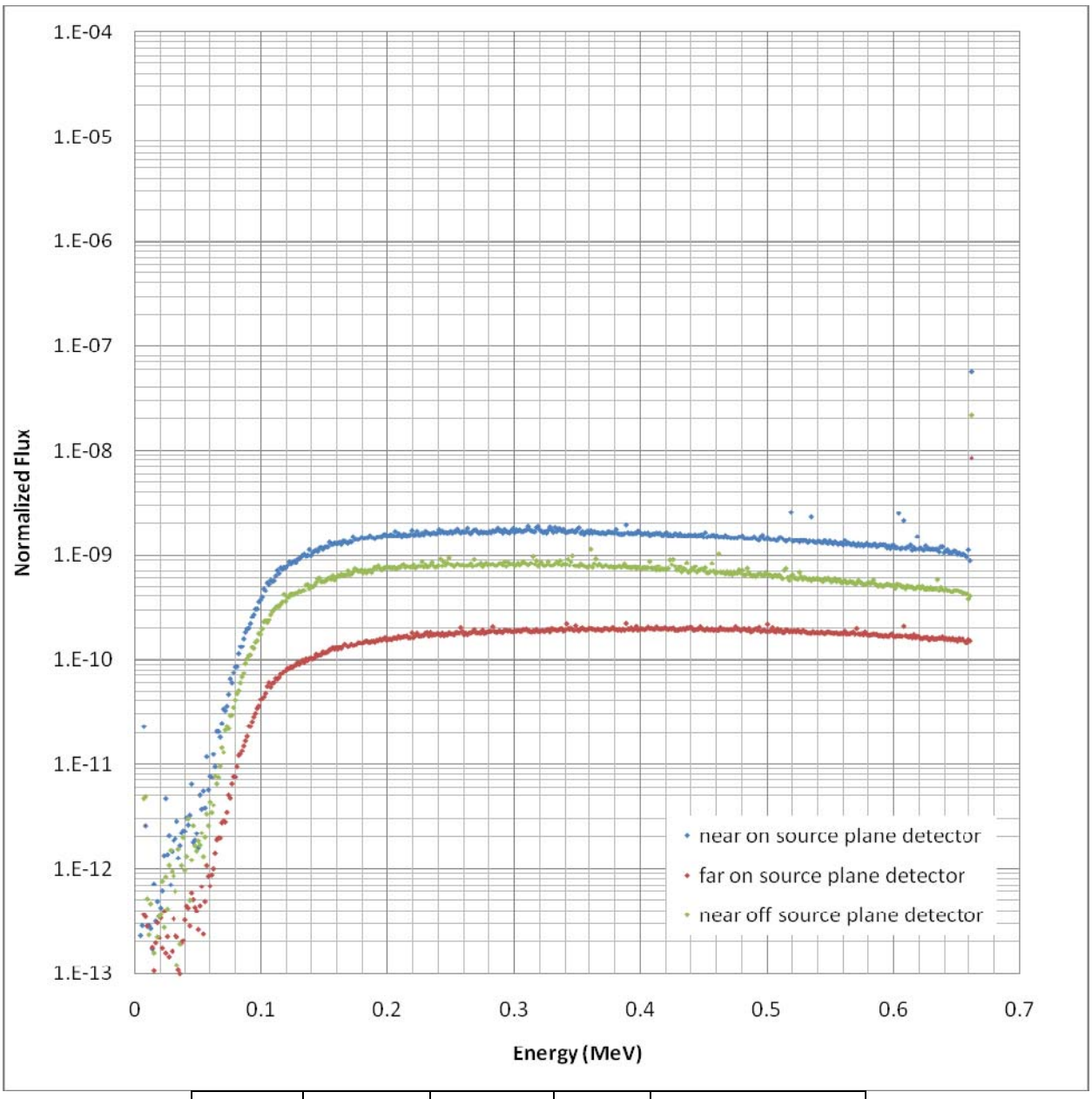

	Isotope	Material	Overpack	Source	Density (g/cm^3)
14	Cs-137	Air	Yes	Point	0.001292

	Collided Area	Sigma	Uncollided Area	Sigma	Ratio	Sigma
near on source plane	1.95E-07	1.42E-09	2.75E-08	1.72E-09	0.14	0.009
far on source plane	2.86E-08	1.11E-10	2.71E-09	1.57E-10	0.095	0.006
near off source plane	8.52E-08	5.03E-10	1.95E-08	1.45E-09	0.23	0.017

Figure 3.16: Results for run 14

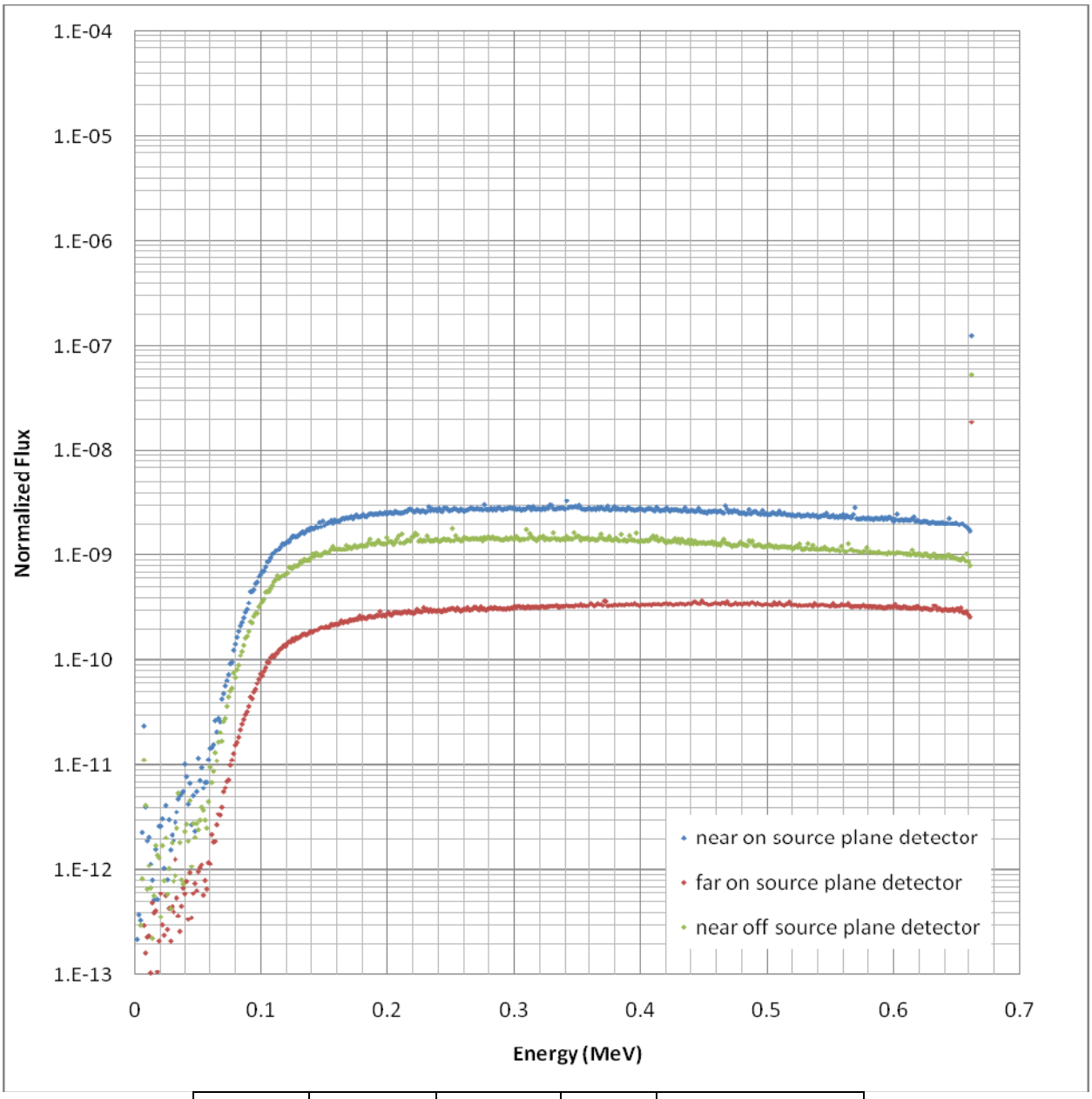

	Isotope	Material	Overpack	Source	Density (g/cm^3)
15	Cs-137	Hydrogen	Yes	Point	0.1

	Collided Area	Sigma	Uncollided Area	Sigma	Ratio	Sigma
near on source plane	1.04E-06	1.58E-09	1.25E-07	4.39E-10	0.120	0.0005
far on source plane	1.27E-07	1.38E-10	1.85E-08	7.78E-11	0.145	0.0006
near off source plane	5.25E-07	1.13E-09	5.22E-08	3.03E-10	0.099	0.0006

Figure 3.17: Results for run 15

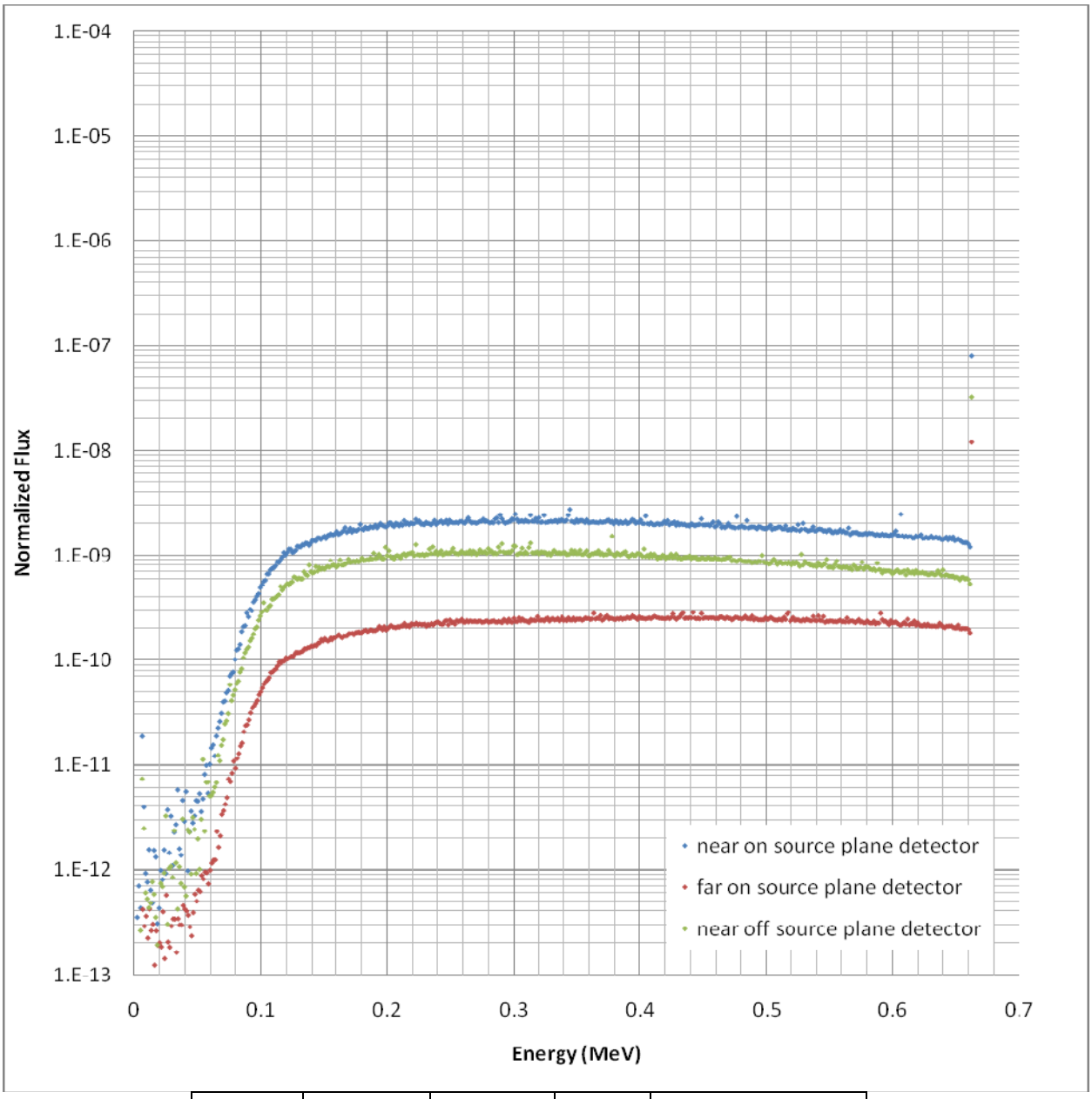

	Isotope	Material	Overpack	Source	Density (g/cm^3)
16	Cs-137	Hydrogen	Yes	Point	0.2

	Collided Area	Sigma	Uncollided Area	Sigma	Ratio	Sigma
near on source plane	7.80E-07	1.81E-09	8.12E-08	3.74E-10	0.104	0.0005
far on source plane	9.41E-08	1.57E-10	1.20E-08	8.29E-11	0.128	0.0009
near off source plane	3.75E-07	1.00E-09	3.19E-08	1.53E-10	0.085	0.0005

Figure 3.18: Results for run 16

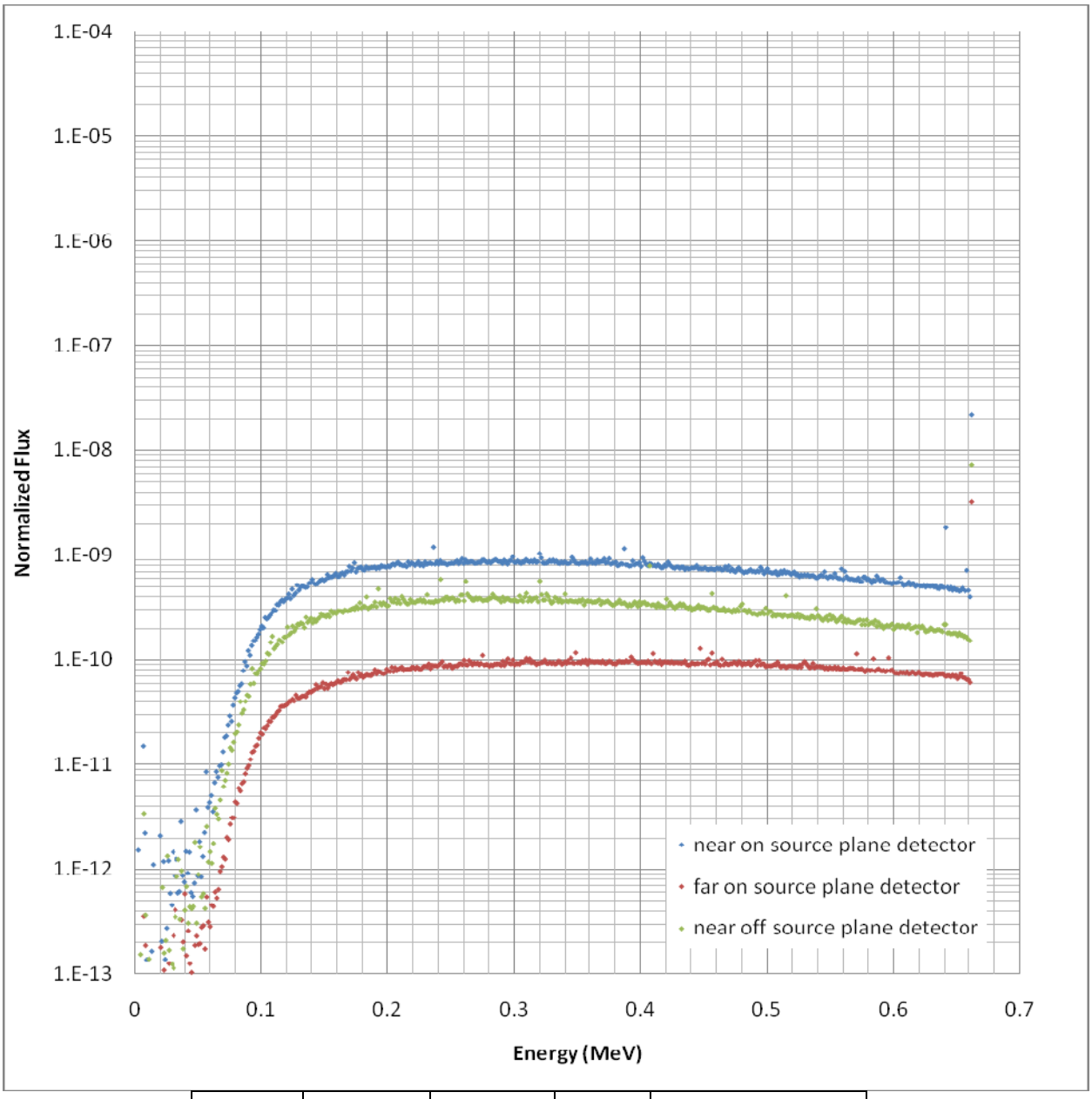

	Isotope	Material	Overpack	Source	Density (g/cm^3)
17	Cs-137	Hydrogen	Yes	Point	0.5

	Collided Area	Sigma	Uncollided Area	Sigma	Ratio	Sigma
near on source plane	3.02E-07	1.57E-09	2.17E-08	1.04E-10	0.072	0.0005
far on source plane	3.48E-08	8.57E-11	3.19E-09	1.15E-11	0.092	0.0004
near off source plane	1.27E-07	6.67E-10	7.27E-09	3.20E-11	0.057	0.0004

Figure 3.19: Results for run 17

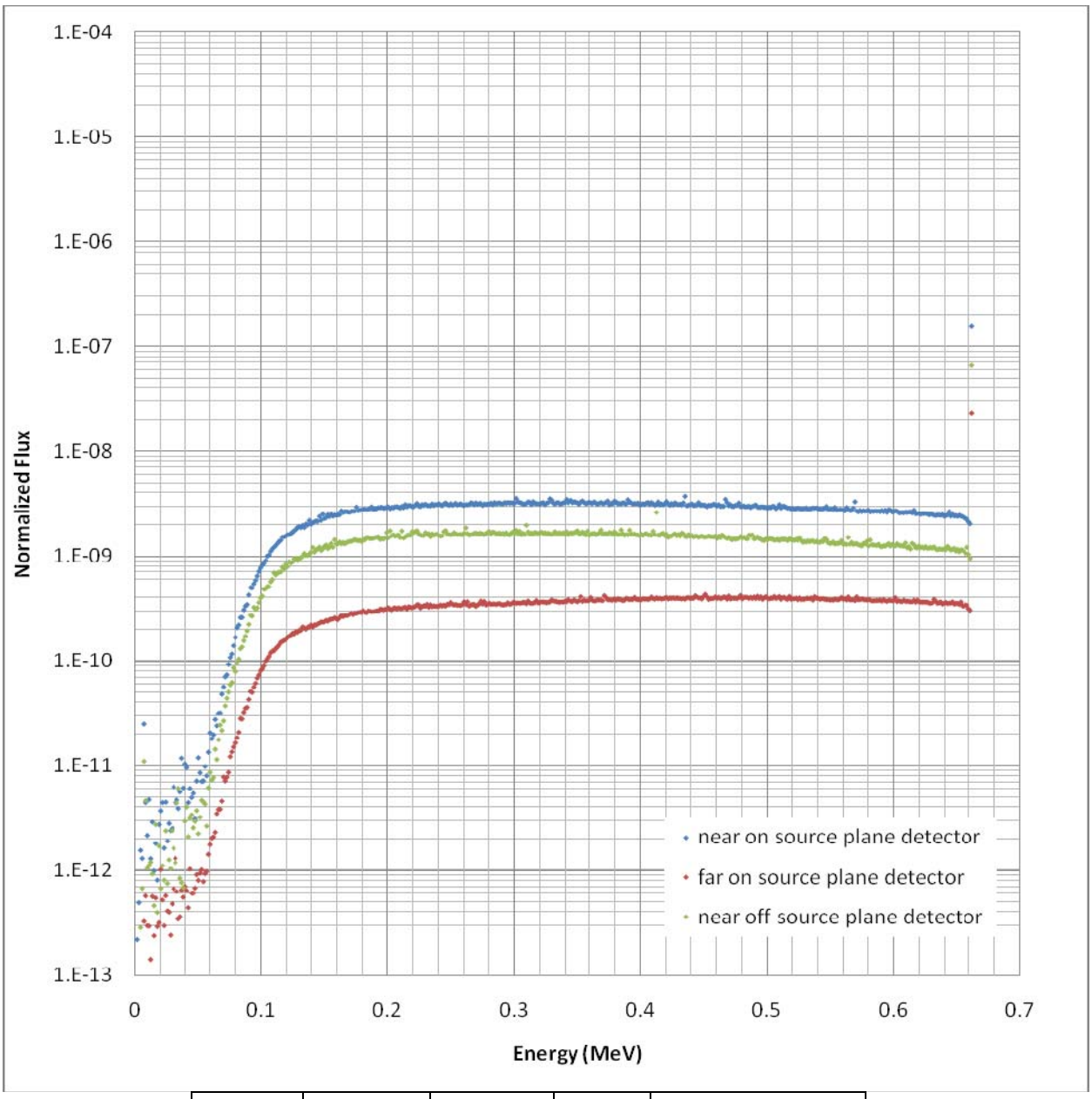

	Isotope	Material	Overpack	Source	Density (g/cm^3)
18	Cs-137	Carbon	Yes	Point	0.1

	Collided Area	Sigma	Uncollided Area	Sigma	Ratio	Sigma
near on source plane	1.20E-06	1.59E-09	1.56E-07	4.82E-10	0.130	0.0004
far on source plane	1.48E-07	1.53E-10	2.30E-08	1.06E-10	0.156	0.0007
near off source plane	6.16E-07	1.38E-09	6.65E-08	3.39E-10	0.108	0.0006

Figure 3.20: Results for run 18

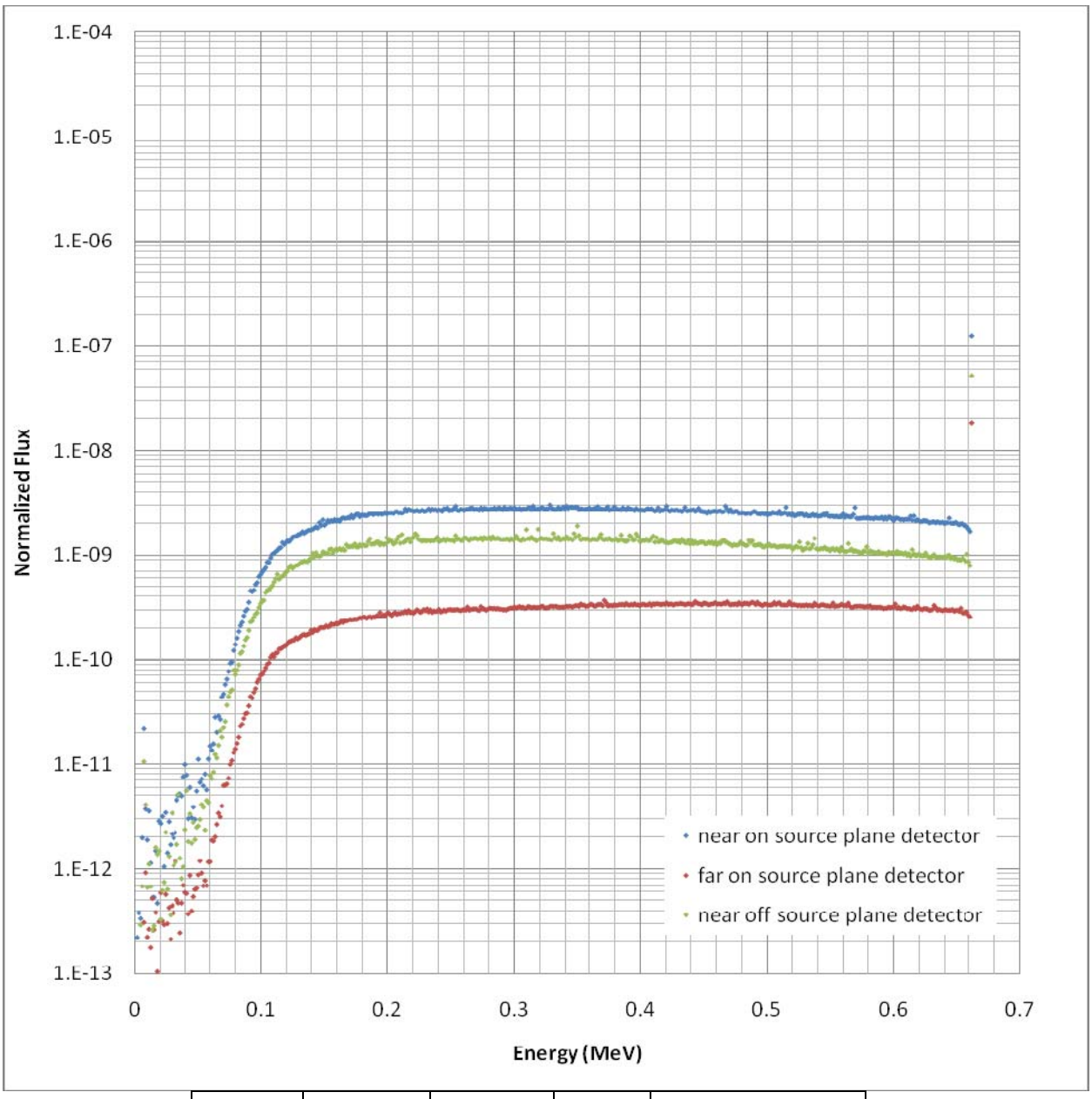

	Isotope	Material	Overpack	Source	Density (g/cm^3)
19	Cs-137	Carbon	Yes	Point	0.2

	Collided Area	Sigma	Uncollided Area	Sigma	Ratio	Sigma
near on source plane	1.04E-06	1.52E-09	1.25E-07	4.37E-10	0.120	0.0005
far on source plane	1.27E-07	1.31E-10	1.85E-08	7.75E-11	0.145	0.0006
near off source plane	5.24E-07	1.21E-09	5.20E-08	3.02E-10	0.099	0.0006

Figure 3.21: Results for run 19

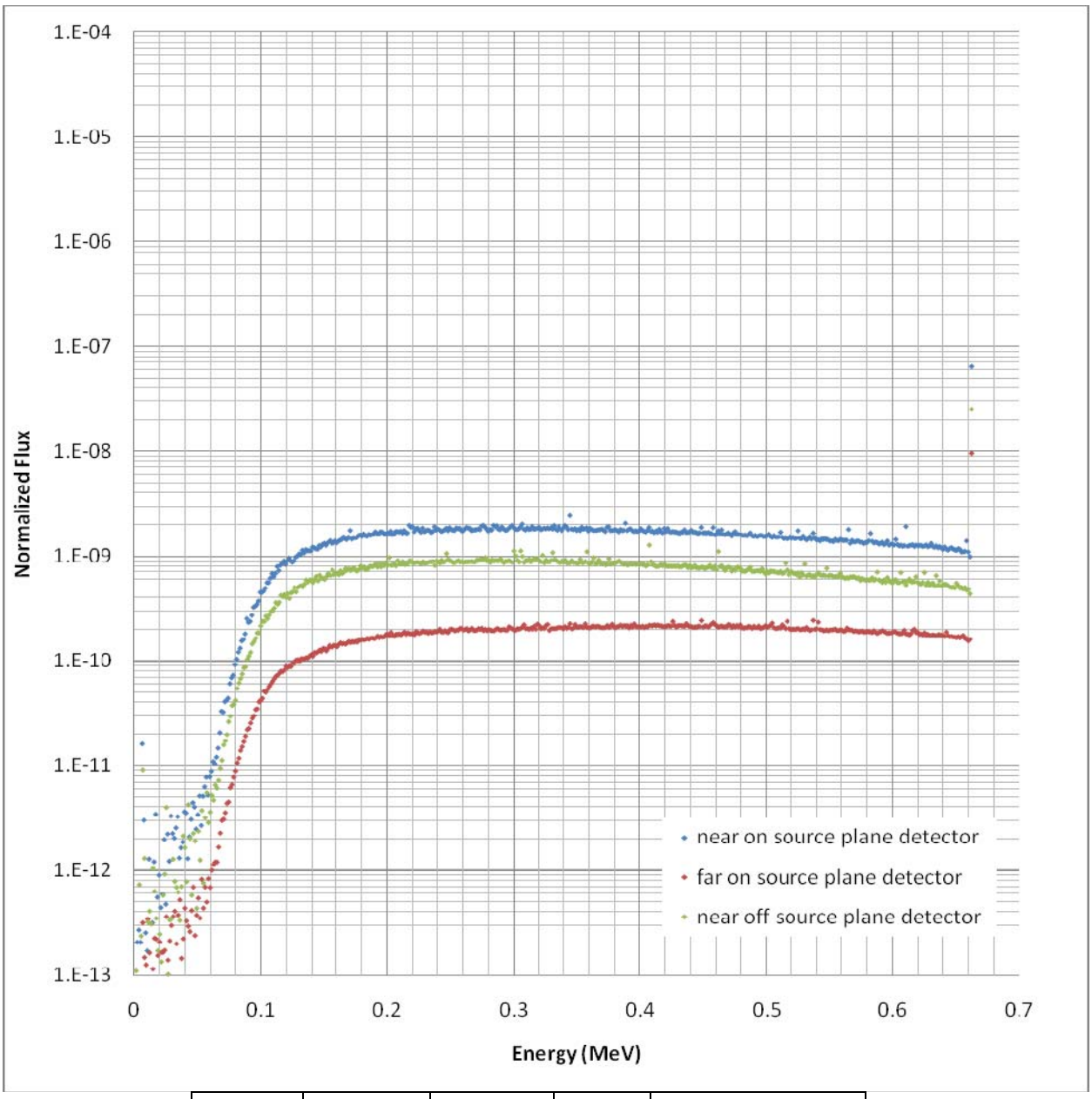

	Isotope	Material	Overpack	Source	Density (g/cm^3)
20	Cs-137	Carbon	Yes	Point	0.5

	Collided Area	Sigma	Uncollided Area	Sigma	Ratio	Sigma
near on source plane	6.66E-07	1.57E-09	6.50E-08	3.64E-10	0.098	0.0006
far on source plane	7.95E-08	1.17E-10	9.60E-09	8.26E-11	0.121	0.0011
near off source plane	3.13E-07	9.57E-10	2.49E-08	1.52E-10	0.079	0.0005

Figure 3.22: Results for run 20

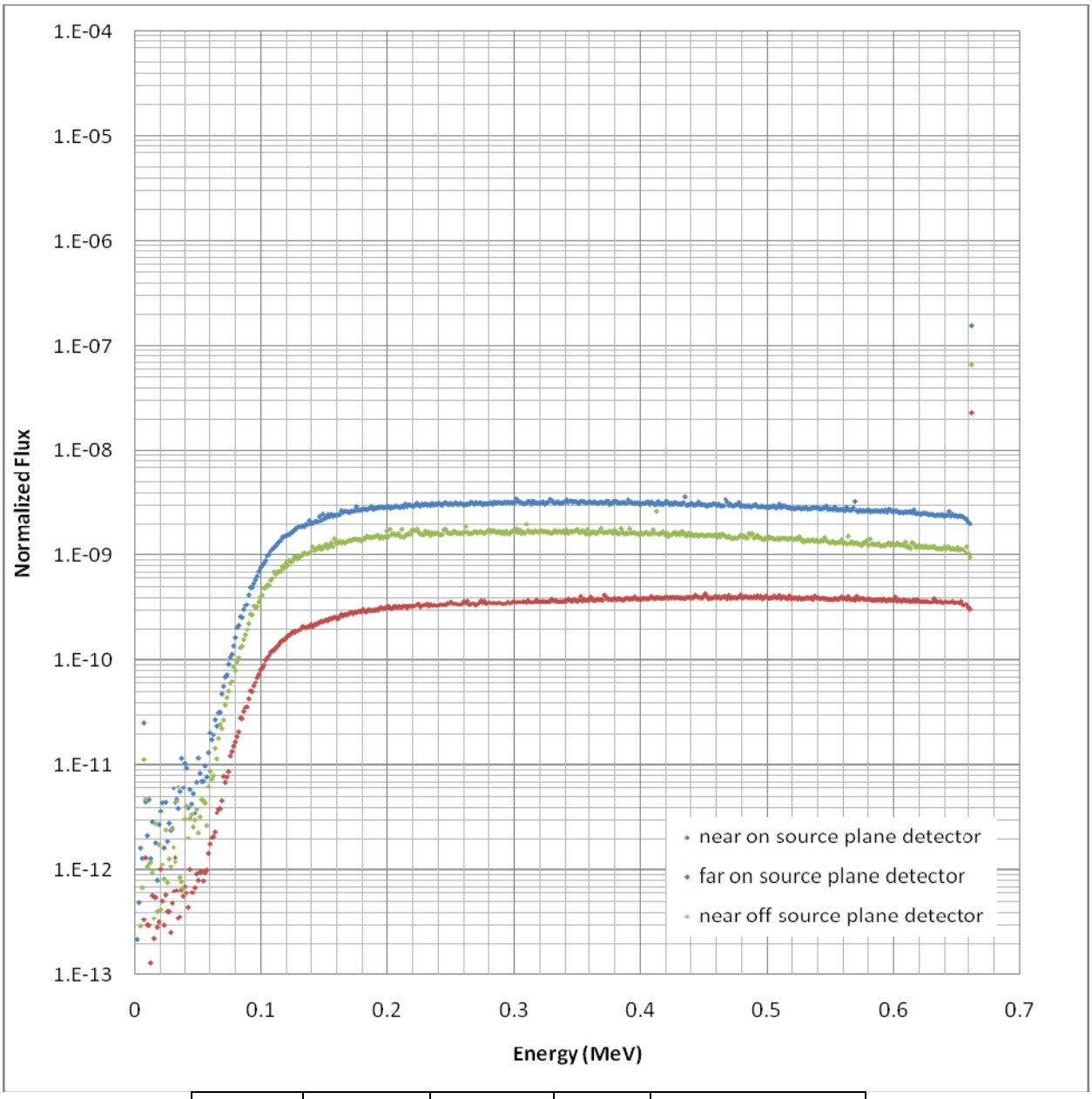

	Isotope	Material	Overpack	Source	Density (g/cm^3)
21	Cs-137	Oxygen	Yes	Point	0.1

	Collided Area	Sigma	Uncollided Area	Sigma	Ratio	Sigma
near on source plane	1.20E-06	1.59E-09	1.56E-07	4.82E-10	0.130	0.0004
far on source plane	1.48E-07	1.53E-10	2.30E-08	1.06E-10	0.156	0.0007
near off source plane	6.16E-07	1.37E-09	6.65E-08	3.39E-10	0.108	0.0006

Figure 3.23: Results for run 21

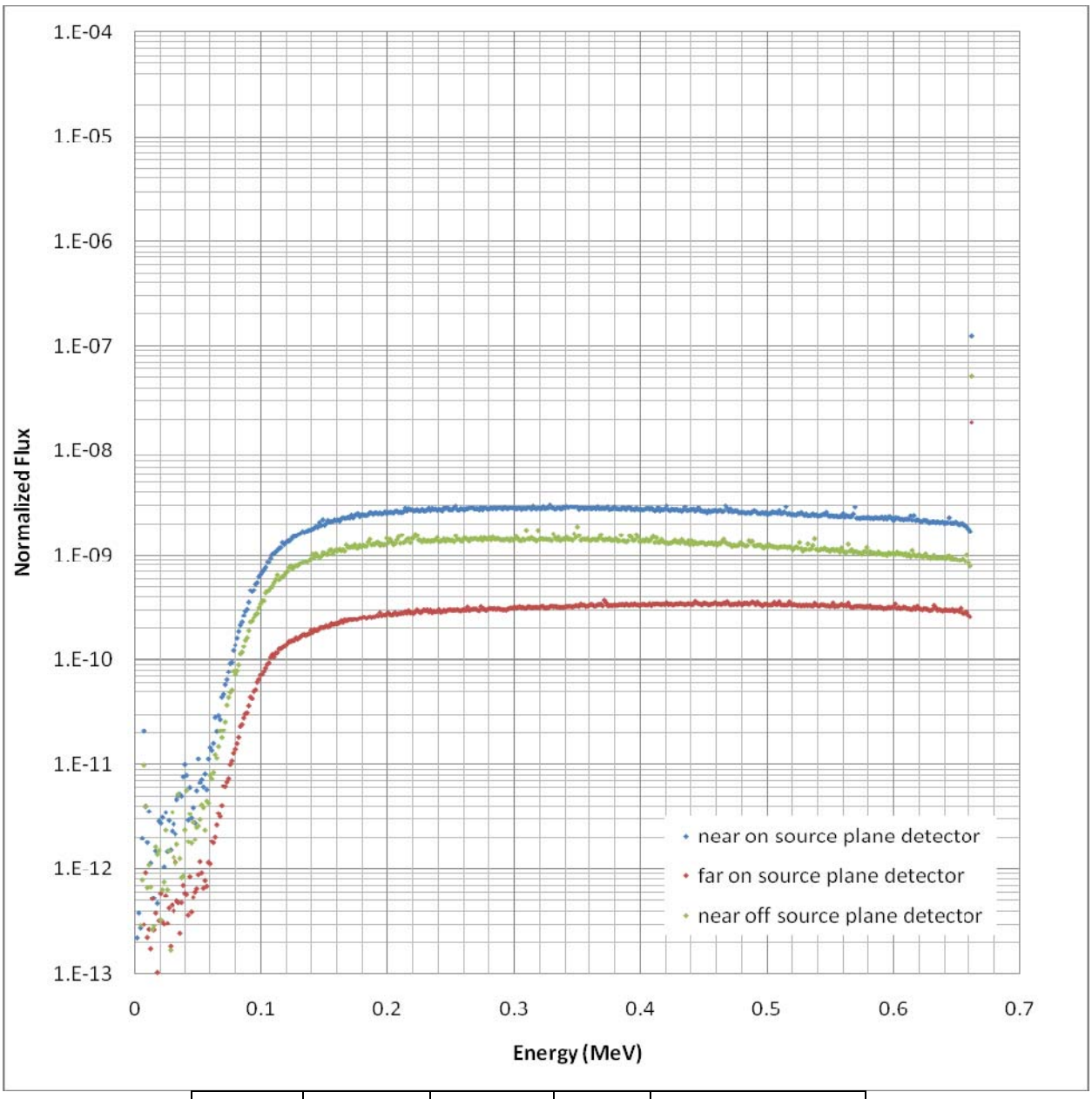

	Isotope	Material	Overpack	Source	Density (g/cm^3)
22	Cs-137	Oxygern	Yes	Point	0.2

	Collided Area	Sigma	Uncollided Area	Sigma	Ratio	Sigma
near on source plane	1.04E-06	1.53E-09	1.25E-07	4.37E-10	0.120	0.0005
far on source plane	1.27E-07	1.31E-10	1.85E-08	7.75E-11	0.145	0.0006
near off source plane	5.24E-07	1.20E-09	5.20E-08	3.01E-10	0.099	0.0006

Figure 3.24: Results for run 22

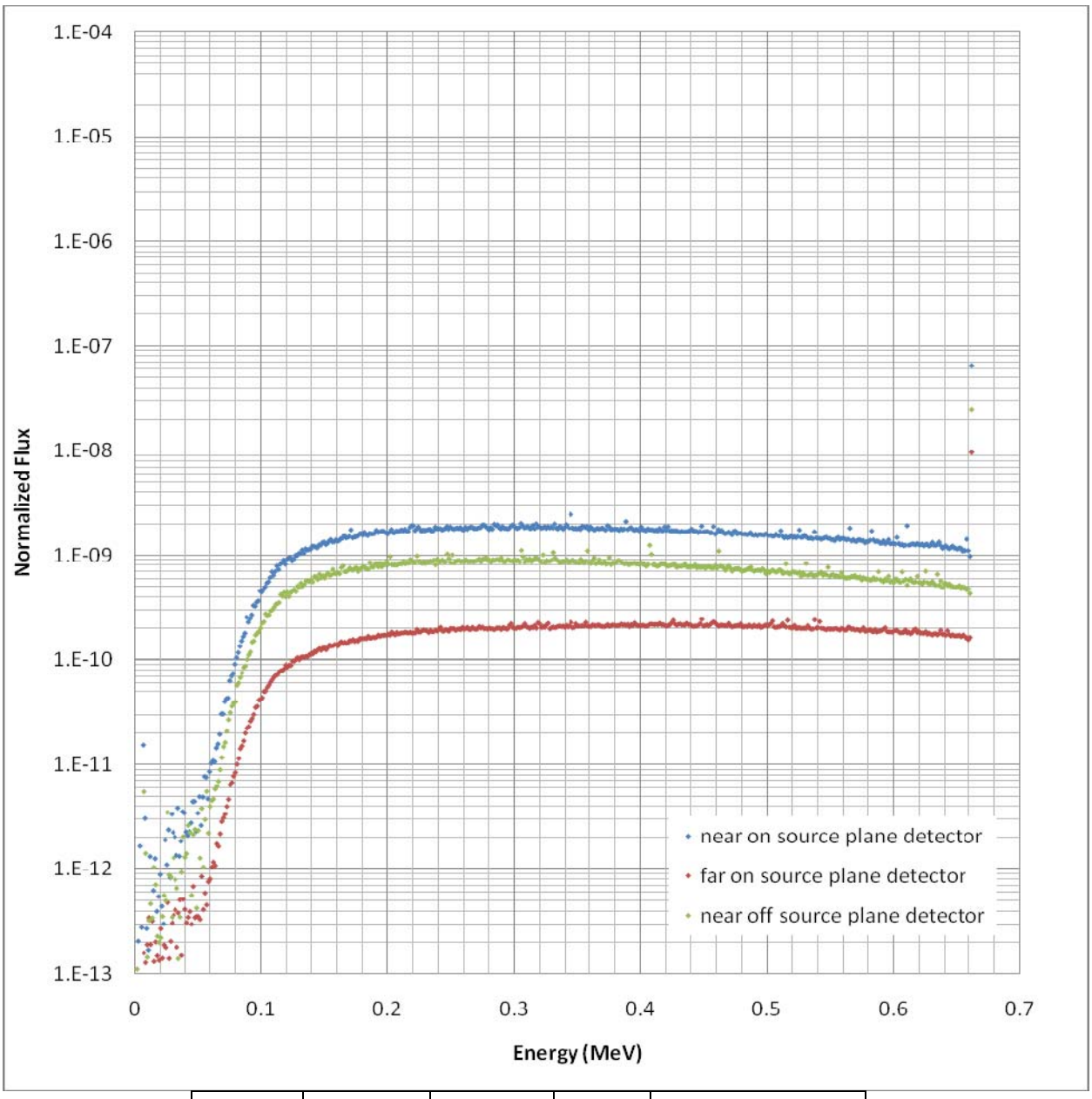

	Isotope	Material	Overpack	Source	Density (g/cm^3)
23	Cs-137	Oxygen	Yes	Point	0.5

	Collided Area	Sigma	Uncollided Area	Sigma	Ratio	Sigma
near on source plane	6.64E-07	1.54E-09	6.48E-08	3.63E-10	0.098	0.0006
far on source plane	7.95E-08	1.19E-10	9.56E-09	6.31E-11	0.120	0.0008
near off source plane	3.13E-07	9.51E-10	2.48E-08	1.41E-10	0.079	0.0005

Figure 3.25: Results for run 23

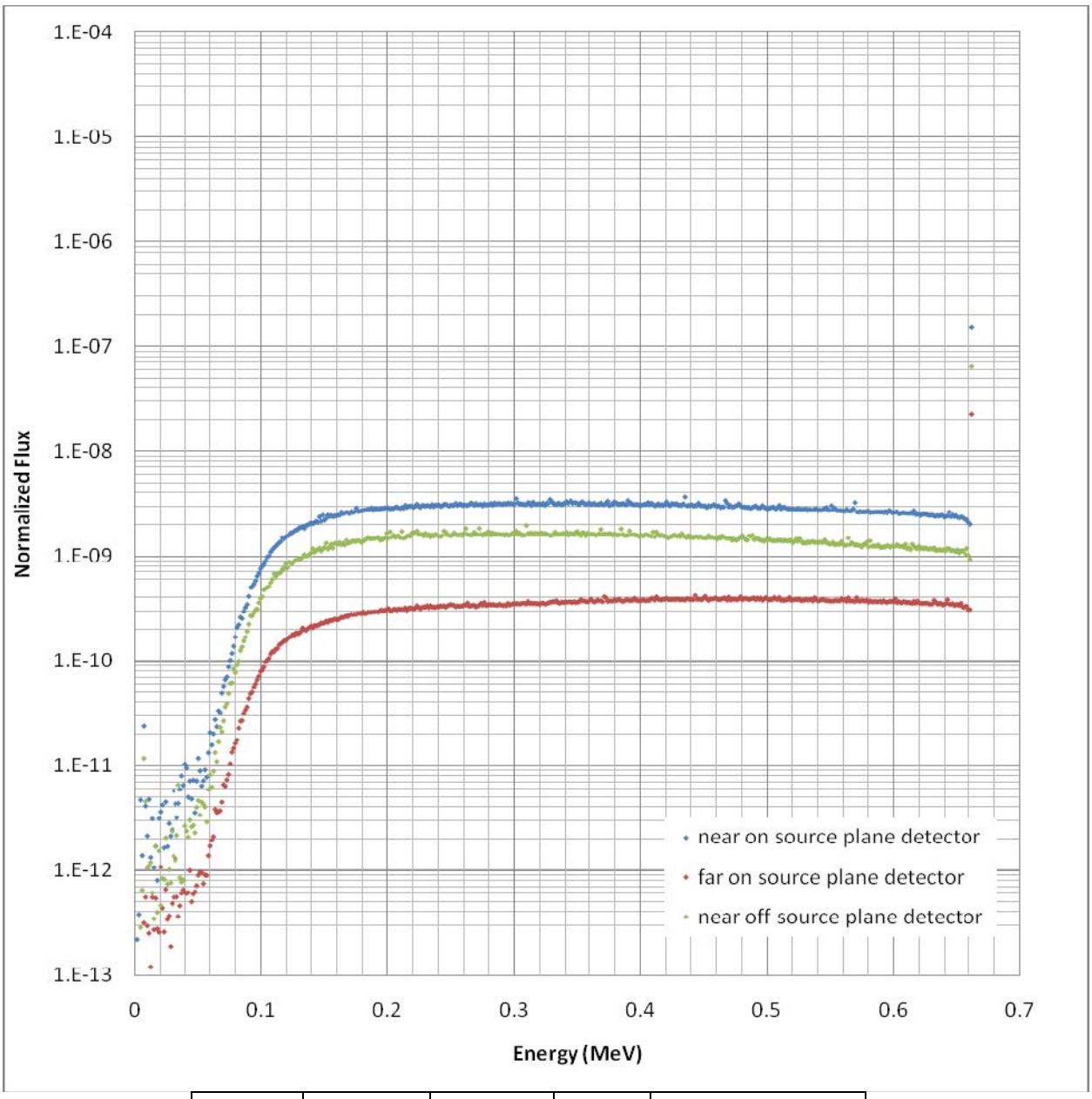

	Isotope	Material	Overpack	Source	Density (g/cm^3)
24	Cs-137	Best Est.	Yes	Point	0.1

	Collided Area	Sigma	Uncollided Area	Sigma	Ratio	Sigma
near on source plane	1.18E-06	1.60E-09	1.52E-07	4.56E-10	0.129	0.0004
far on source plane	1.45E-07	1.52E-10	2.25E-08	1.06E-10	0.155	0.0007
near off source plane	6.05E-07	1.07E-09	6.49E-08	3.37E-10	0.107	0.0006

Figure 3.26: Results for run 24

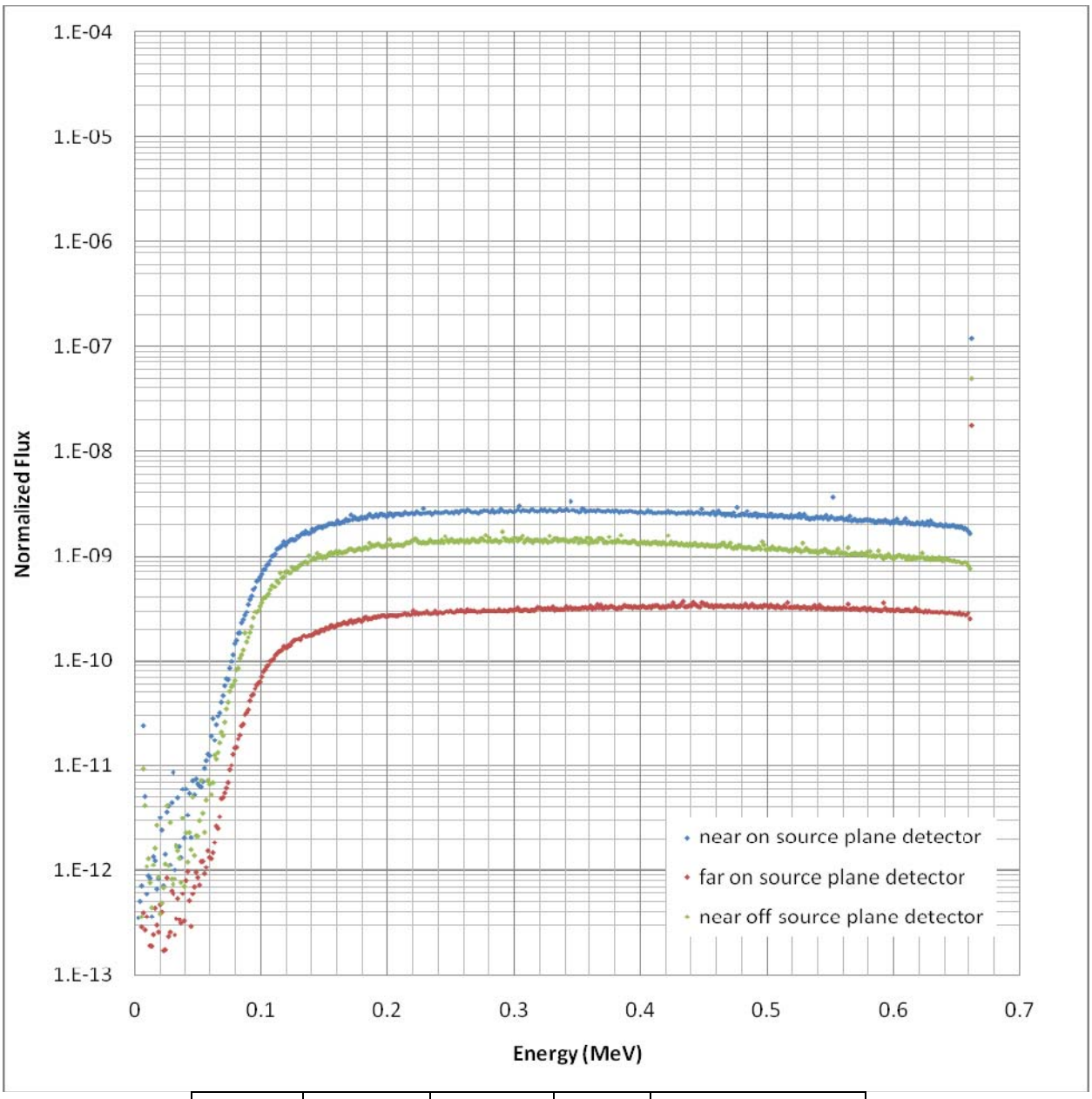

	Isotope	Material	Overpack	Source	Density (g/cm^3)
25	Cs-137	Best Est.	Yes	Point	0.2

	Collided Area	Sigma	Uncollided Area	Sigma	Ratio	Sigma
near on source plane	1.01E-06	2.06E-09	1.19E-07	6.09E-10	0.118	0.0006
far on source plane	1.24E-07	1.51E-10	1.76E-08	7.57E-11	0.142	0.0006
near off source plane	5.05E-07	9.63E-10	4.96E-08	3.77E-10	0.098	0.0008

Figure 3.27: Results for run 25

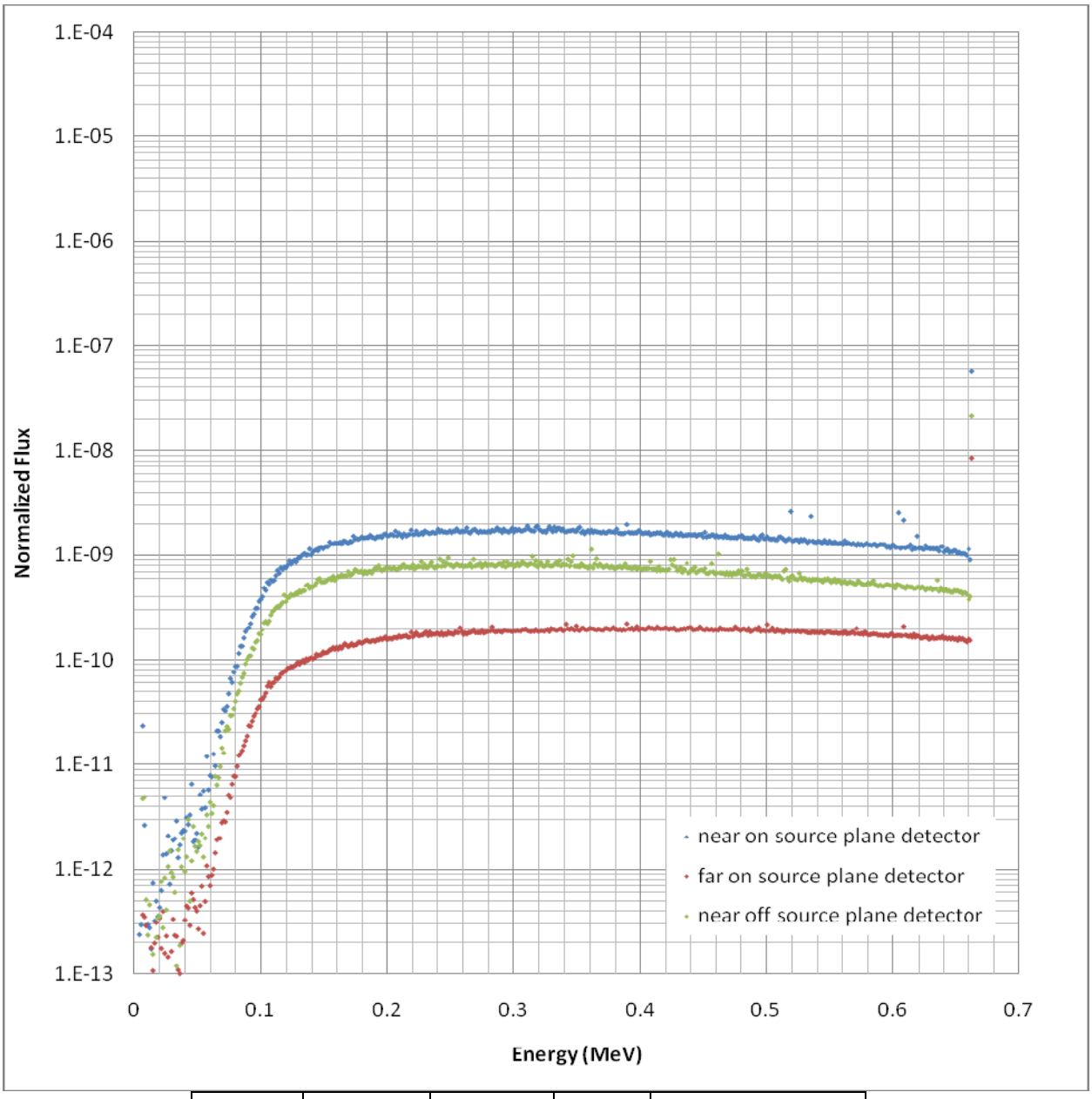

	Isotope	Material	Overpack	Source	Density (g/cm^3)
26	Cs-137	Best Est.	Yes	Point	0.5

	Collided Area	Sigma	Uncollided Area	Sigma	Ratio	Sigma
near on source plane	6.15E-07	2.51E-09	5.74E-08	2.18E-10	0.093	0.0005
far on source plane	7.28E-08	1.05E-10	8.43E-09	2.70E-11	0.116	0.0004
near off source plane	2.85E-07	8.04E-10	2.18E-08	1.88E-10	0.077	0.0007

Figure 3.28: Results for run 26

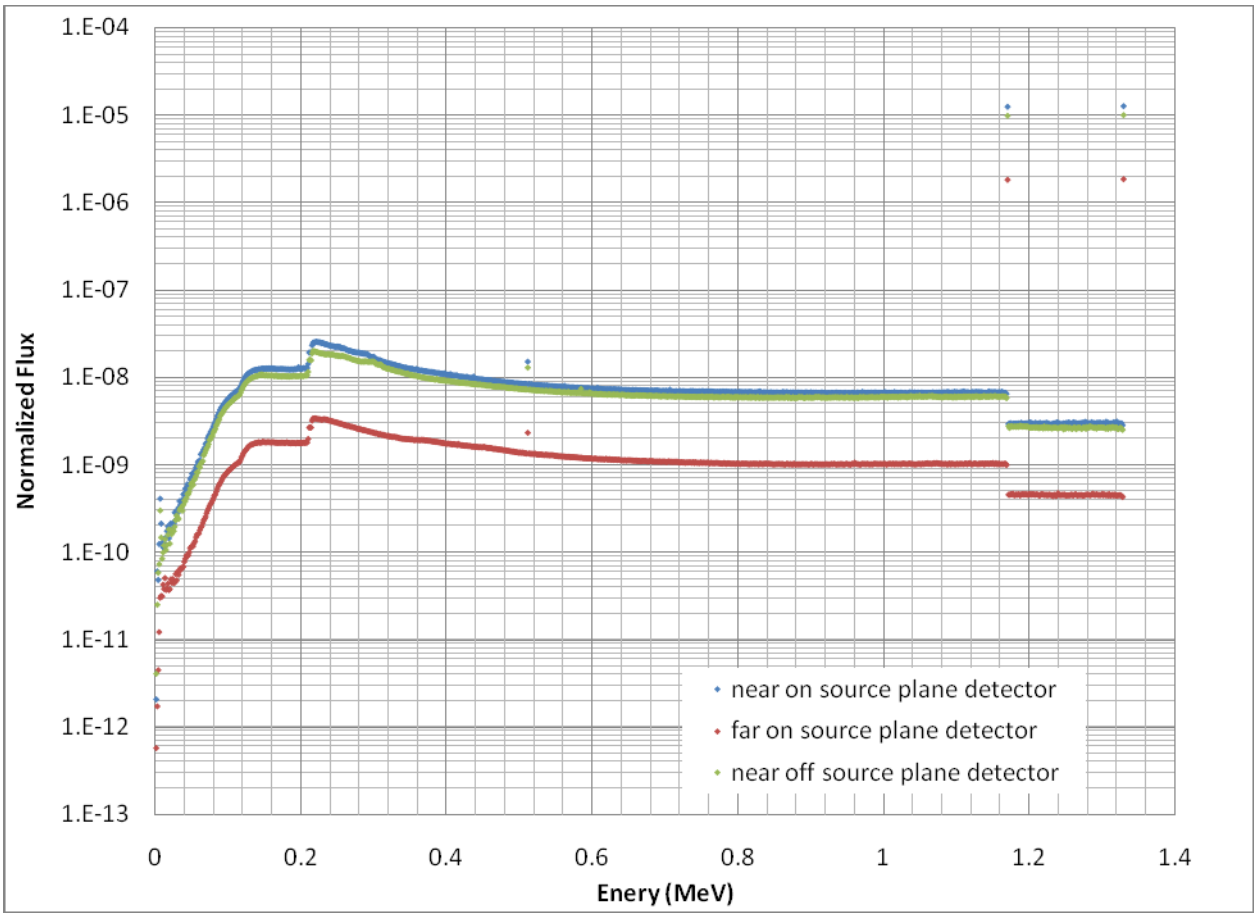

	Isotope	Material	Overpack	Source	Density (g/cm^3)
27	Co-60	Best Est.	No	Point	0.1

	collided flux	sigma	lower uncollided	sigma	upper uncollided	sigma
near on source plane	8.11E-06	2.08E-09	1.24E-05	1.24E-09	1.26E-05	1.26E-09
far on source plane	1.22E-06	2.47E-10	1.83E-06	1.83E-10	1.86E-06	1.86E-10
near off source plane	6.82E-06	1.90E-09	9.67E-06	2.90E-09	9.83E-06	9.83E-10

	lower to collided	sigma	upper to collided	sigma
near on source plane	1.53	0.0003	1.56	0.0003
far on source plane	1.50	0.0002	1.52	0.0002
near off source plane	1.42	0.0004	1.44	0.0003

Figure 3.29: Results for run 27

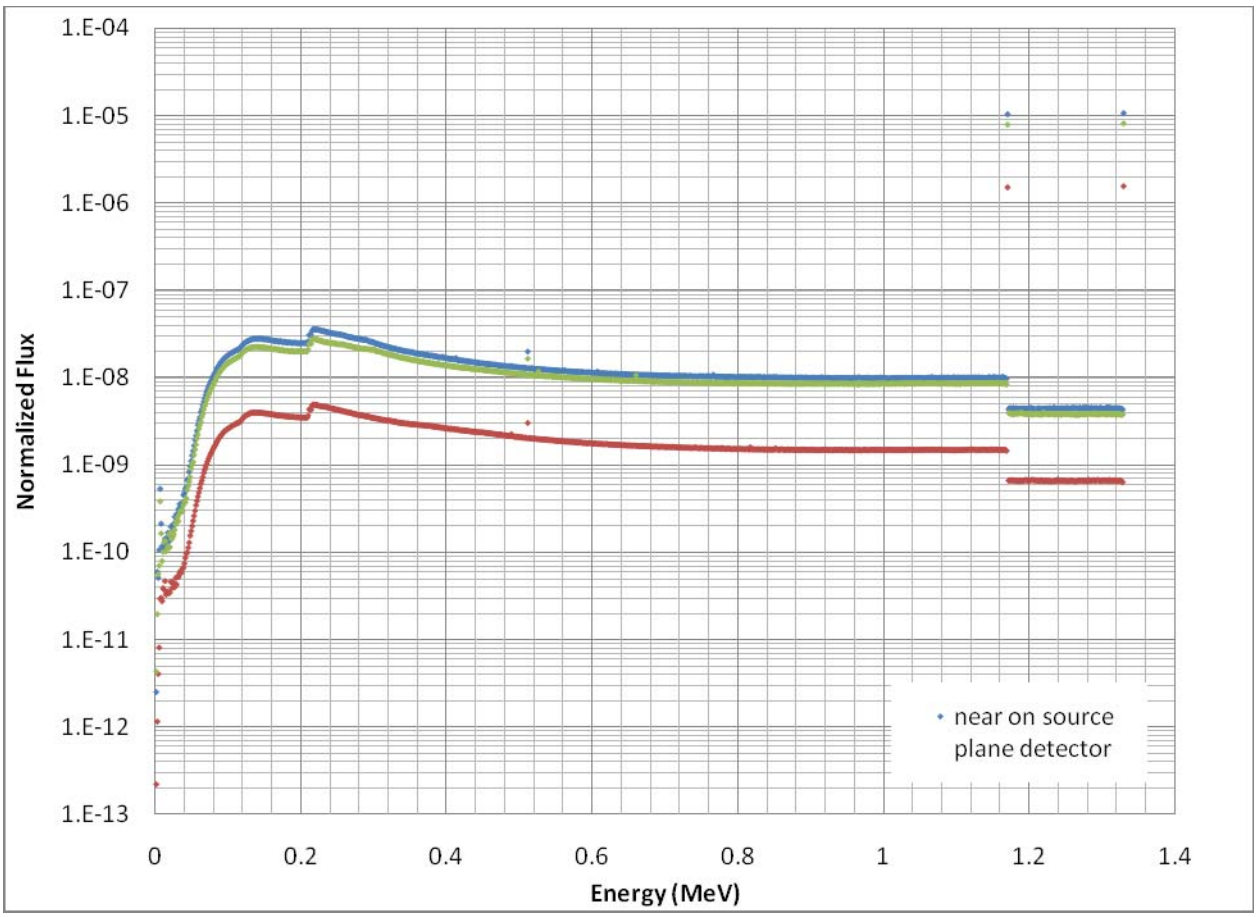

	Isotope	Material	Overpack	Source	Density (g/cm^3)
28	Co-60	Best Est.	No	Point	0.2

	collided flux	sigma	lower uncollided	sigma	upper uncollided	sigma
near on source plane	1.29E-05	2.62E-09	1.03E-05	1.03E-09	1.06E-05	1.06E-09
far on source plane	1.93E-06	3.45E-10	1.52E-06	3.04E-10	1.56E-06	1.56E-10
near off source plane	1.06E-05	2.85E-09	7.87E-06	2.36E-09	8.11E-06	4.05E-09

	lower to collided	sigma	upper to collided	sigma
near on source plane	0.80	0.0002	0.82	0.0002
far on source plane	0.79	0.0003	0.81	0.0002
near off source plane	0.74	0.0004	0.76	0.0006

Figure 3.30: Results for run 28

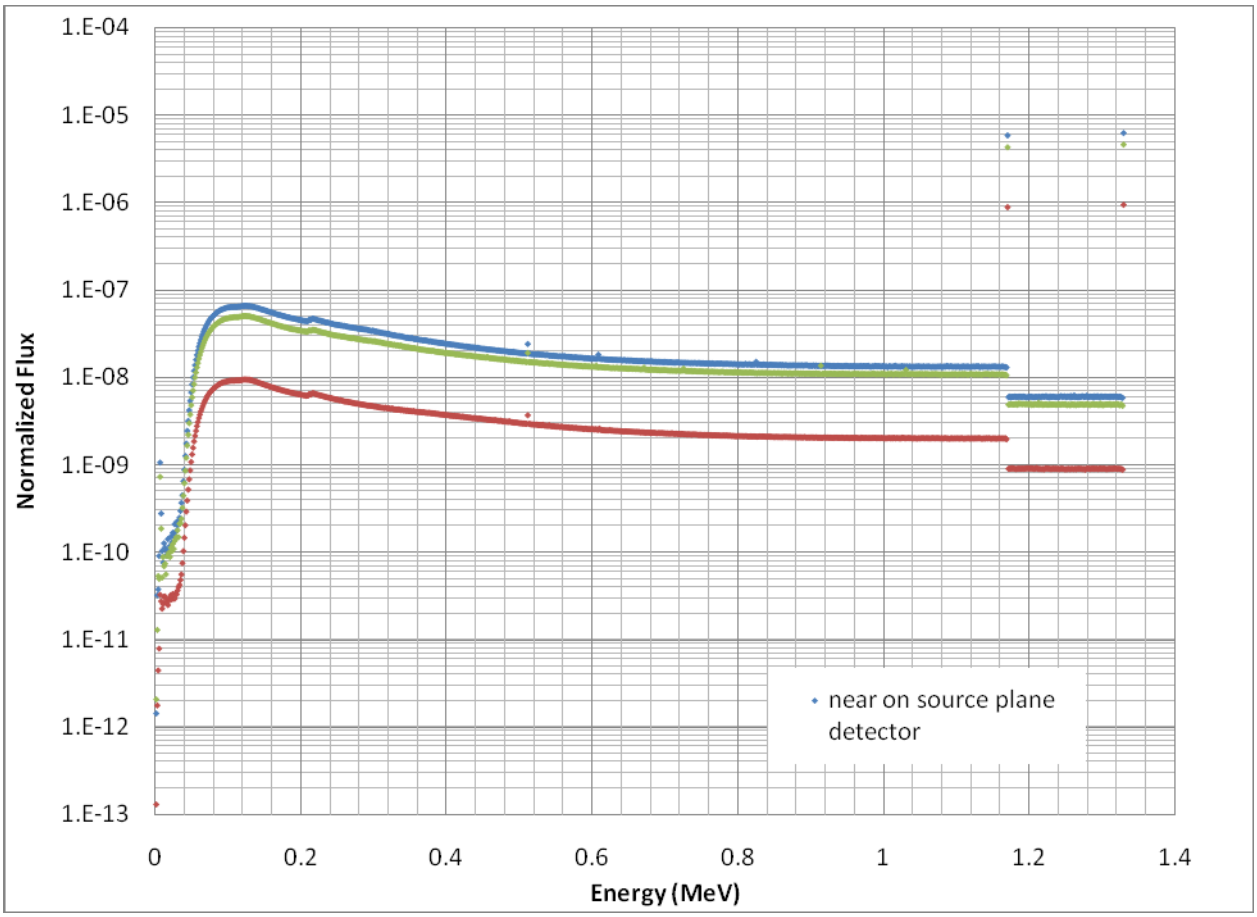

	Isotope	Material	Overpack	Source	Density (g/cm^3)
29	Co-60	Best Est.	No	Point	0.5

	collided flux	sigma	lower uncollided	sigma	upper uncollided	sigma
Near on source plane	3.33E-05	3.94E-09	5.94E-06	5.94E-10	6.32E-06	6.32E-10
far on source plane	4.86E-06	4.19E-10	8.74E-07	1.75E-10	9.30E-07	9.30E-11
near off source plane	2.49E-05	4.31E-09	4.23E-06	1.27E-09	4.54E-06	1.81E-09

	lower to collided	sigma	upper to collided	sigma
Near on source plane	0.18	0.0002	0.19	0.0002
far on source plane	0.18	0.0002	0.19	0.0001
near off source plane	0.17	0.0003	0.18	0.0004

Figure 3.31 Results for run 29

3.4.2 Impact of the waste matrix composition selection

Results obtained for the 4 considered waste matrix composition (hydrogen only, carbon only, oxygen only, and a realistic best-estimate mix) are shown in Fig 3.32, in all cases for density 0.2 g/cm^3. Results for hydrogen are about one third lower in the peak area, and about 40% higher for the collided area. However, the "hydrogen only" composition is very unrealistic. The maximum differences between the other 3 cases are less than 10%. That means, the sensitivity to the exact composition is low, and the best estimate composition may be safely used to produce accurate results.

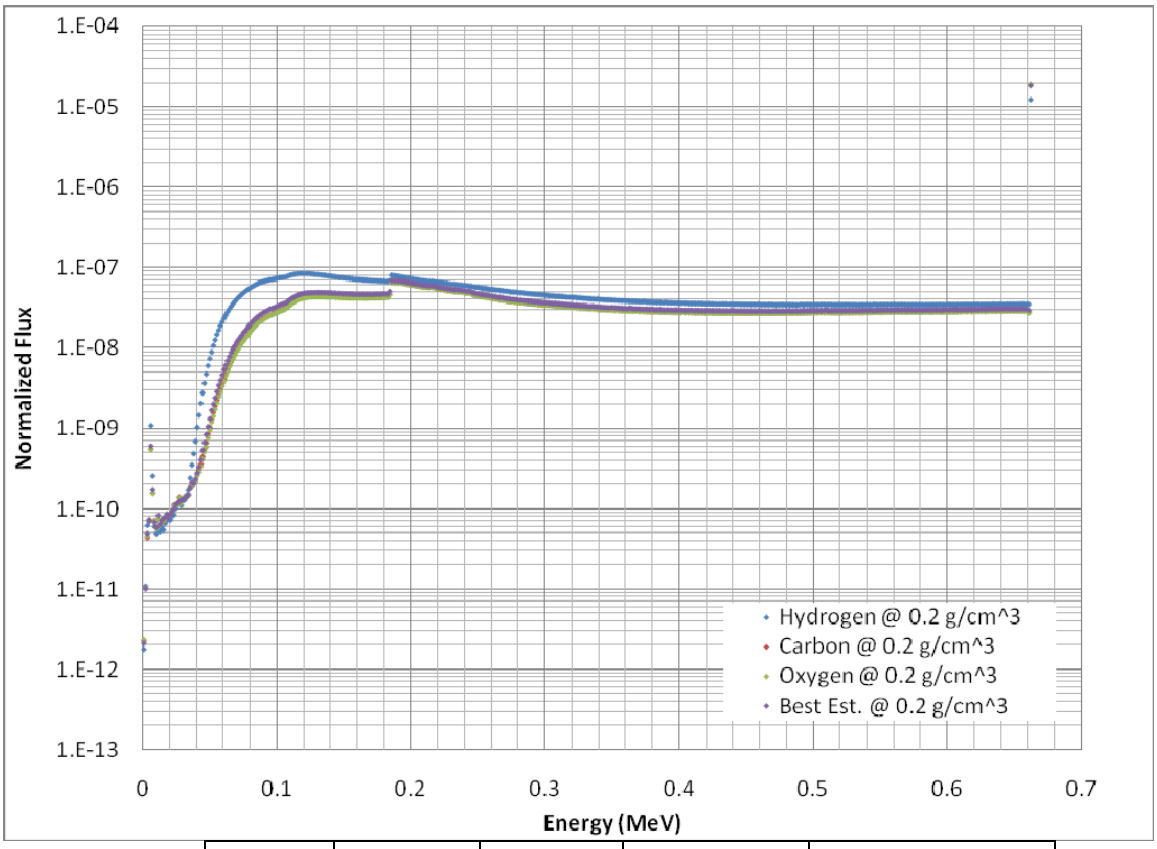

	Isotope	Material	Overpack	Source	Density (g/cm^3)
3	Cs-137	Hydrogen	No	Point	0.2
6	Cs-137	Carbon	No	Point	0.2
9	Cs-137	Oxygen	No	Point	0.2
12	Cs-137	Best Est.	No	Point	0.2

	Collided Area	Sigma	Uncollided Area	Sigma	Ratio	Sigma
near on source plane	2.16E-05	3.04E-09	1.23E-05	2.46E-09	0.568	0.0001
near on source plane	1.51E-05	2.71E-09	1.89E-05	3.78E-09	1.250	0.0003
near on source plane	1.51E-05	2.97E-09	1.89E-05	3.78E-09	1.250	0.0004
near on source plane	1.61E-05	2.85E-09	1.81E-05	3.62E-09	1.127	0.0003

Figure 3.32 Impact of the waste matrix composition

3.4.3 Impact of the waste matrix density

The estimated typical density in actual waste drums is ~0.2 g/cm^3, which was selected as the reference density. To evaluate impact of the waste matrix density variability, simulations were performed for two additional densities, one higher and one lower, i.e., 0.1 and 0.5 g/cm^3, bounding the range of expected cases. Results obtained for these 3 densities assumed for the best estimate composition are shown in Fig. 3.33. (Note that results were generated also for other waste matrix compositions and variable density, documented in Section 3.3, but only the best estimate composition is analyzed here.)

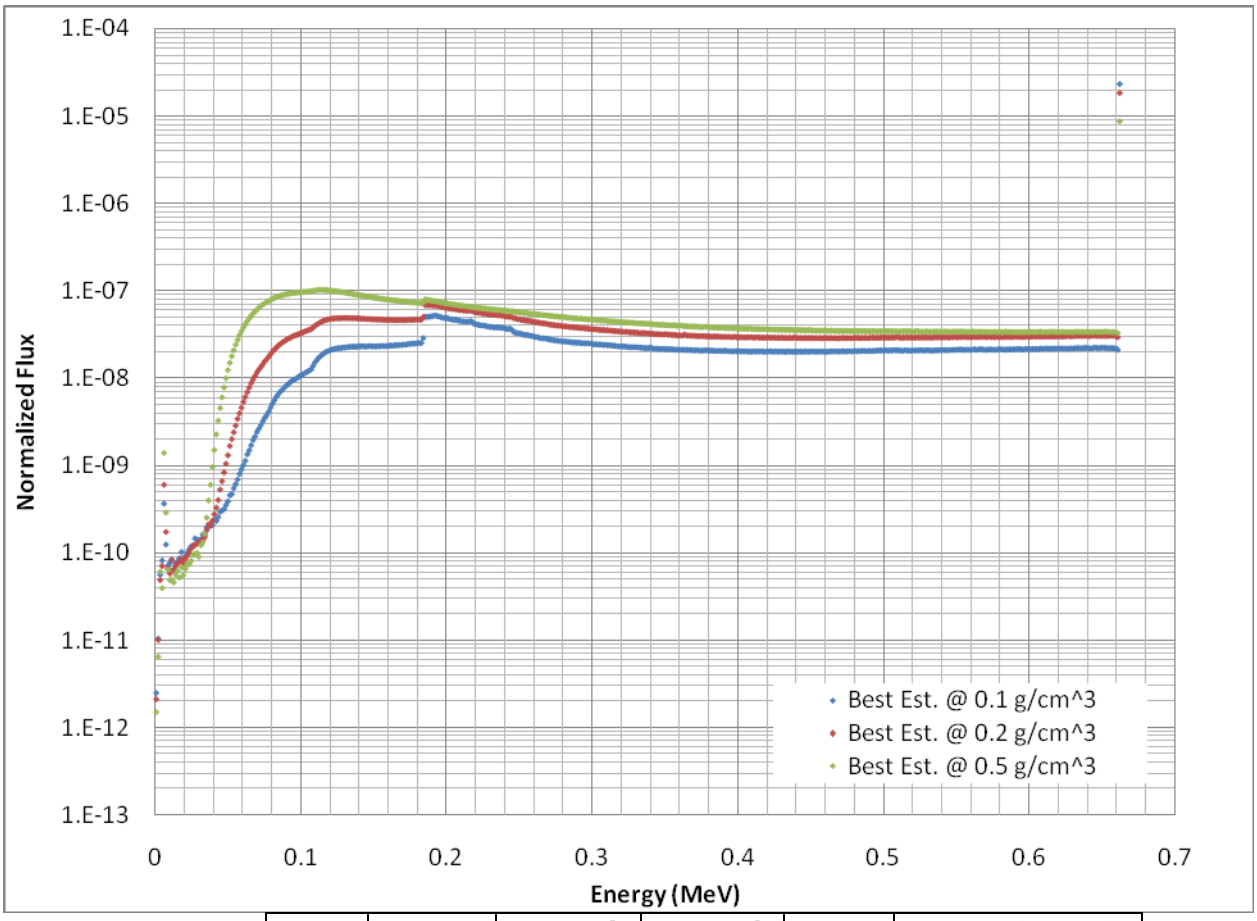

	Isotope	Material	Overpack	Source	Density (g/cm^3)
11	Cs-137	Best Est.	No	Point	0.1
12	Cs-137	Best Est.	No	Point	0.2
13	Cs-137	Best Est.	No	Point	0.5

	Collided Area	Sigma	Uncollided Area	Sigma	Ratio	Sigma
near on source plane	1.04E-05	2.29E-09	2.30E-05	2.30E-09	2.211	0.0005
near on source plane	1.61E-05	2.85E-09	1.81E-05	3.62E-09	1.127	0.0003
near on source plane	2.32E-05	3.60E-09	8.75E-06	2.62E-09	0.377	0.0001

Figure 3.33 Impact of the waste matrix density

As expected, a higher/lower density will decrease/increase the peak area, in this case by a factor of 0.48 and 1.27, respectively. Change of an opposite direction will occur with the collided area. Specific numbers are given in the second table included within Fig. 3.33.

In order to improve usefulness of the obtained data for future unfolding, we consider the following physical characteristics of the photon scattering. For cesium source and photon energy of 662 keV, the maximum energy loss (if not absorption) in first collision occurs for backscattering at 180 deg, to energy of ~184 keV. Thus, higher density of the waste matrix promotes multiple scattering, but at the same time attenuates more. One could then expect that the collided area below 184 keV will relatively increase compared to the collided area above 185 keV.

Such effect is in fact observed, as shown in spectra in Fig 3.33 and numerically in Table 3.2. The ratio of the two collided areas provides a new information/parameter that may be used in future unfolding to adequately treat the density effect, due to its increased sensitivity to the density. The change of the uncollided area with density, for the two energy sub-regions is shown in Fig. 3.34.

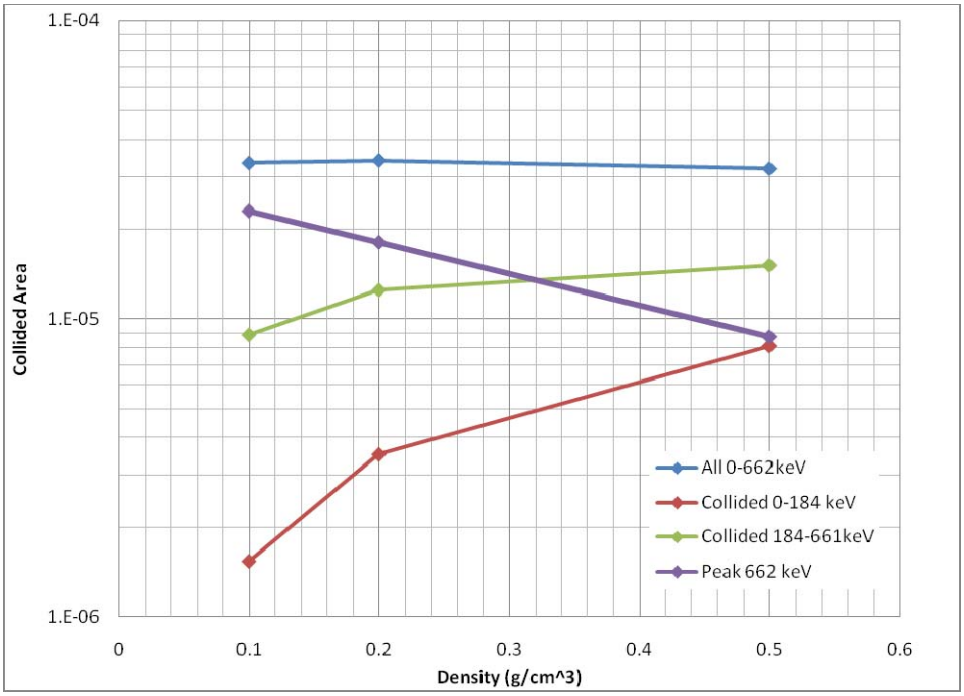

Figure 3.34 Impact of the waste matrix density on energy regions in collided area

Density (g/cm^3)	0-184 keV	Sigma	185-661 keV	Sigma	Fraction *	Sigma
0.1	1.54E-06	8.23E-10	8.88E-06	2.13E-09	0.148	0.0006
0.2	3.51E-06	1.28E-09	1.25E-05	2.55E-09	0.219	0.0004
0.5	8.10E-06	2.02E-09	1.51E-05	2.98E-09	0.350	0.0003

* - fraction = ratio of low to total collided, i.e.: (0-184 keV) / (0-661 keV)

Table 3.2: Impact of the waste matrix density on the collided area

3.4.4 Impact of the Source Energy (Cobalt Source)

The waste matrix density effect on spectra in the case of cobalt source is shown in Fig. 3.35. The table now includes data for two peaks (upper and lower uncollided). Due to the dual source energy, there is a step in the collided spectrum; additionally, the higher source energy, shifts the backscattered energy to above 200 keV. Table 3.3 presents ratios of the areas depending on the waste matrix density.

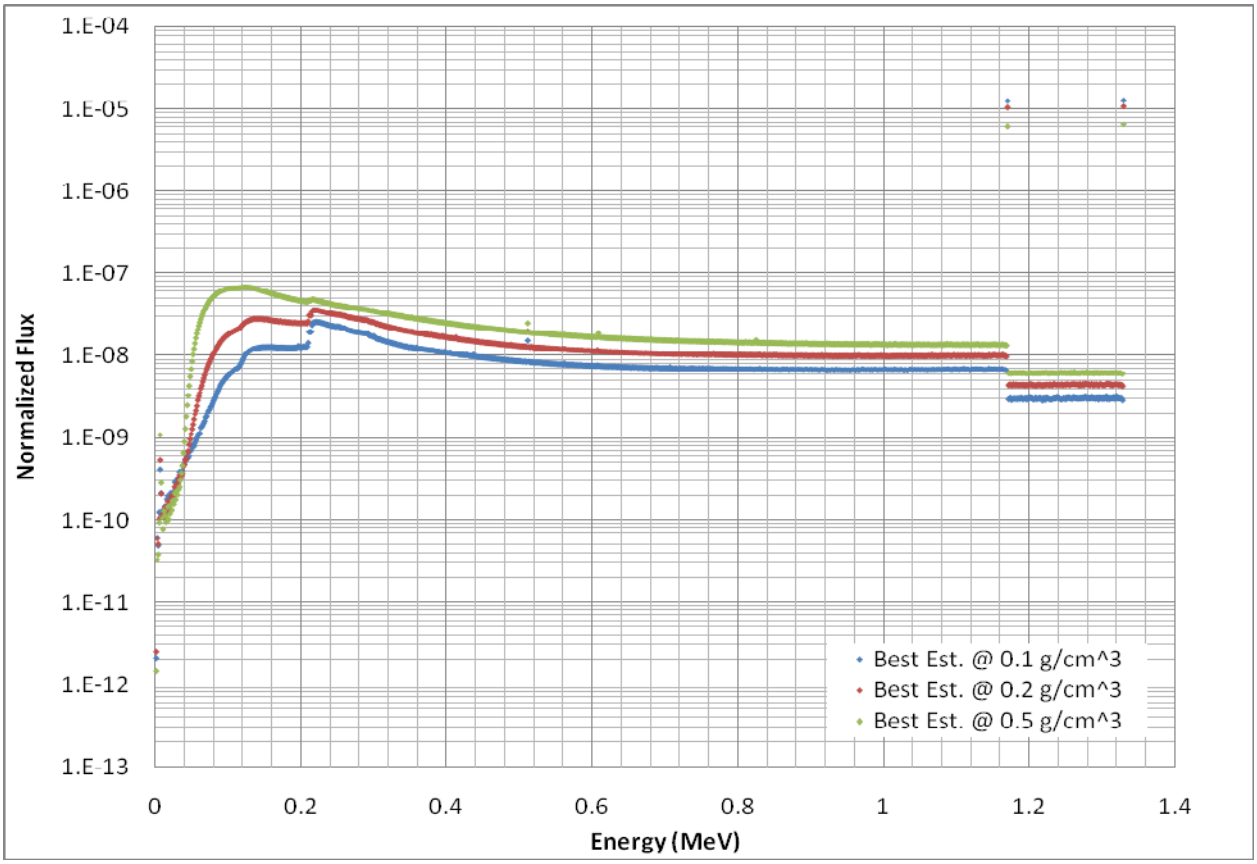

	Isotope	Material	Overpack	Source	Density (g/cm^3)
27	Co-60	Best Est.	No	Point	0.1
28	Co-60	Best Est.	No	Point	0.2
29	Co-60	Best Est.	No	Point	0.5

	collided flux	sigma	lower uncollided	sigma	upper uncollided	sigma
near on source plane	8.11E-06	2.08E-09	1.24E-05	1.24E-09	1.26E-05	1.26E-09
near on source plane	1.29E-05	2.62E-09	1.03E-05	1.03E-09	1.06E-05	1.06E-09
near on source plane	3.33E-05	3.94E-09	5.94E-06	5.94E-10	6.32E-06	6.32E-10

Figure 3.35 Impact of the waste matrix density for cobalt source

	Density (g/cm^3)	lower to collided	sigma	upper to collided	sigma
near on source plane	0.1	1.53	0.0003	1.56	0.0003
near on source plane	0.2	0.80	0.0002	0.82	0.0002
near on source plane	0.5	0.18	0.0002	0.19	0.0002

Table 3.3: Impact of the waste matrix density for cobalt source

3.4.5 Effect of the overpack

Effect of the overpack on spectrum is shown in Fig. 3.36, which compares results with and without overpack for the best estimate waste matrix composition at 0.2 g/cm^3, with cesium point source.

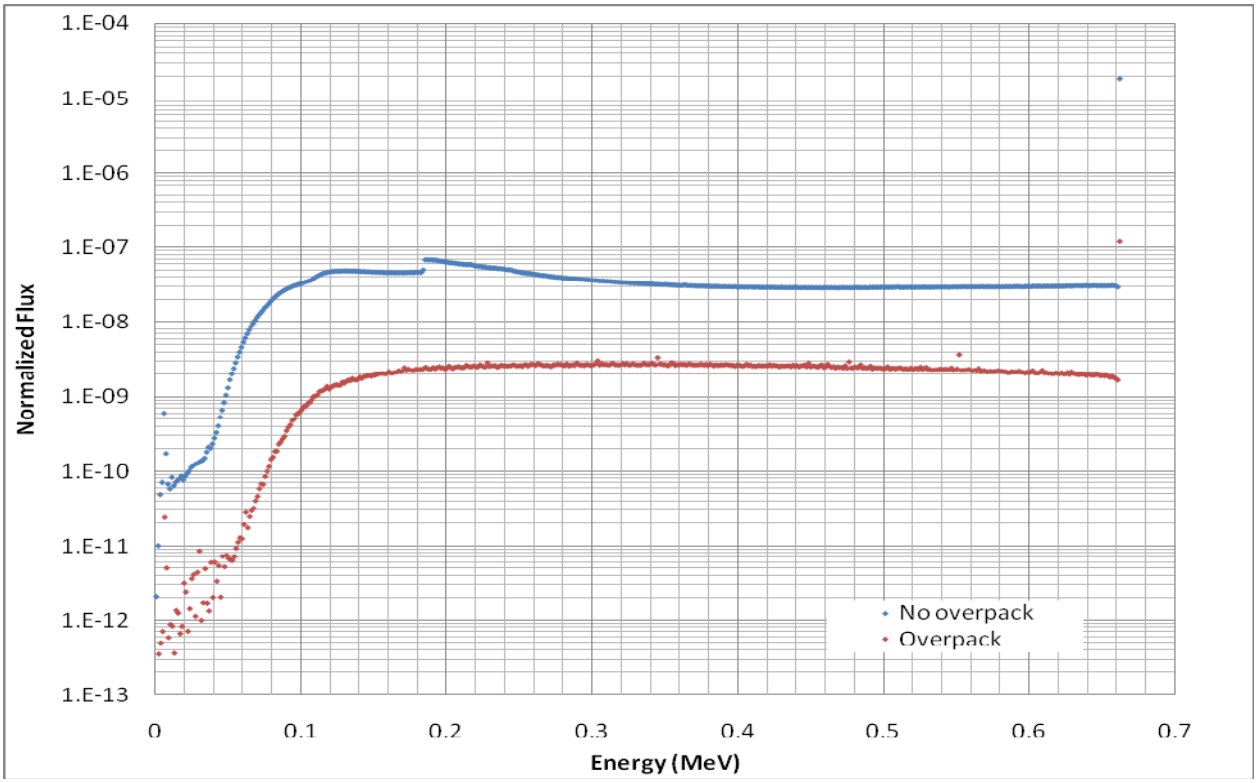

	Isotope	Material	Overpack	Source	Density (g/cm^3)
12	Cs-137	Best Est.	No	Point	0.2
25	Cs-137	Best Est.	Yes	Point	0.2

	Collided Area	Sigma	Uncollided Area	Sigma	Ratio	Sigma
near on source plane	1.61E-05	2.85E-09	1.81E-05	3.62E-09	1.127	0.0003
near on source plane	1.01E-06	2.06E-09	1.19E-07	6.09E-10	0.118	0.0006

Figure 3.36 Impact of the overpack

As expected, the overpack reduced the uncollided area more than the collided area, about two orders of magnitude vs one order of magnitude, respectively. Additionally, it masked or smeared most of specific spectral features. This implies that for unfolding to have a chance of succeeding, it may be necessary to remove the overpack.

3.4.6 Off-Center Source Location

All previous simulations assumed a centered point source. In this section we investigate the impact of off-centered source. Due to the validity of superposition, we again investigate only a single off-center source.

Assuming that measurements are performed on a rotating drum, the rotation will somewhat average the effect of the off-centered source. However, the average detector response for the off-center source will be different than for the same source but centered. Therefore, it would be desirable to determine the approximate source position as part of the future unfolding algorithm.

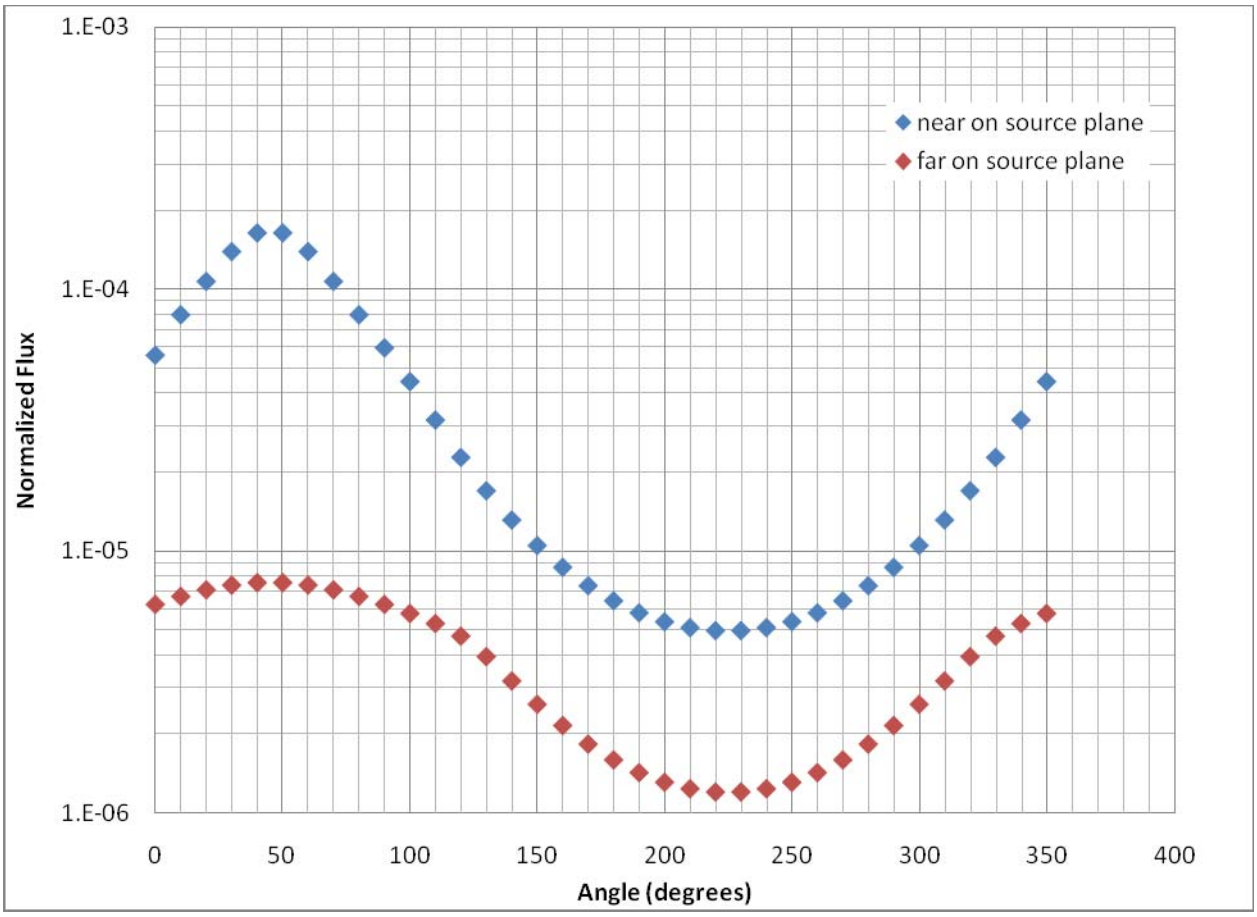

Figure 3.37 Azimuthal detector response for an off-center source

The first step is to consider azimuthal (“angle-gated”) detector response rather than only the average. It is expected to obtain an oscillating curve, representing the periodic change in the source-to-detector distance.

The difficulty is that the amplitude of oscillation will depend both on the distance itself (geometric factor), and attenuation through the waste matrix, which in turn depends on the matrix density. To enhance unfolding, we have considered that two detectors would be available, a closer one, amplifying the geometrical effect, and a farther one, where the geometric effect would be reduced, and oscillations would be due primarily to the different attenuation through the waste matrix. Fig. 3.37 shows responses for the two detectors.

From their different oscillation amplitude, the two “unknowns”, density effect and off-center effect may be better resolved that from a single curve. Further study of how to address multiple off-centered sources is foreseen in future studies.

4. Summary and Conclusions

The performed work addresses the Compton scattering in the waste matrix itself. The related topics of subsequent Compton scattering in the detector, Compton suppression, and unfolding algorithms were outside the scope. In this study, organic waste in 55-gallon drum was considered, with or without an overpack. The reference source was defined to be ^{137}Cs; additionally, ^{60}Co was considered. The "reference case" or "base case" was established, with a representative (best estimate) waste matrix density and composition and the source centered in the drum. A number of "branch cases" were defined where a single or several parameters of the reference case were modified (such as the waste matrix density, source position, etc.), within a realistic range, to investigate their impact on the results. The objective was to evaluate gamma spectra resulting from a mono-energetic gamma source of 662 keV, affected by Compton scattering within the waste drum, as observed outside the waste drum.

MCNP simulations were performed for about 30 cases. The leakage gamma spectra outside the drum were obtained at three selected locations, two of them corresponding to the source axial elevation plane (one closer and one farther away from the drum) and the third one close to the drum but off the source plane. The impact of the Compton scattering within the waste on the spectrum shape, magnitude, and specific features was investigated. The ratio of the unscattered-to-scattered gammas, i.e., peak to total Compton was used as a representative single factor.

The impact of the waste matrix composition was evaluated. The results essentially depend primarily on the matrix bulk density (g/cm^3) and do not differentiate much between the elements such as C, O, and N. Therefore, the best-estimate waste matrix composition is suitable for most analyses, i.e., for a wide variability in the waste matrix composition. The matrix density naturally impacts results. Moreover, we subdivided the collided area into two portions, one above and other below the energy corresponding to backscatter at 180 degrees. The ratio of these two subregions, provides a new parameter sensitive to the density change, which is expected to help in the future unfolding algorithm development.

The overpack, assumed to consist of 3.5" of steel, reduces the uncollided photon flux by about two orders of magnitude and the collided one by one order of magnitude. It also masks/smears most of the spectral features, thus making unfolding of any within drum information rather difficult, without removing the overpack.

In another "branch" study, a radially off-center radiation source was assumed. It was demonstrated that using multiple detectors, for example a close and a far detector, interfering effects of the matrix density and source position may be resolved, and more accurate unfolding of the detector position may be accomplished.

Finally, to provide some bounds on the source energy impact, additional simulations were performed with a different source energy, corresponding to two main cobalt lines.

The presented results are only the first step toward the overall long-term objective of using simulation results coupled with advanced unfolding algorithms to improve filtering out of the Compton-scattering component in the unfolding process. They provide a good basis for further research aimed to improving non-destructive gamma-ray based evaluation methods.

5. References

[1] MCNP — A General Monte Carlo N-Particle Transport Code, Version 5, X-5 Monte Carlo Team, April 24, 2003 LA-UR-03-1987

[2] G.F. Knoll, *Radiation Detection and Measurement*, 2nd ed. John Wiley & Sons, 1979.

App. A

Drum Specifications

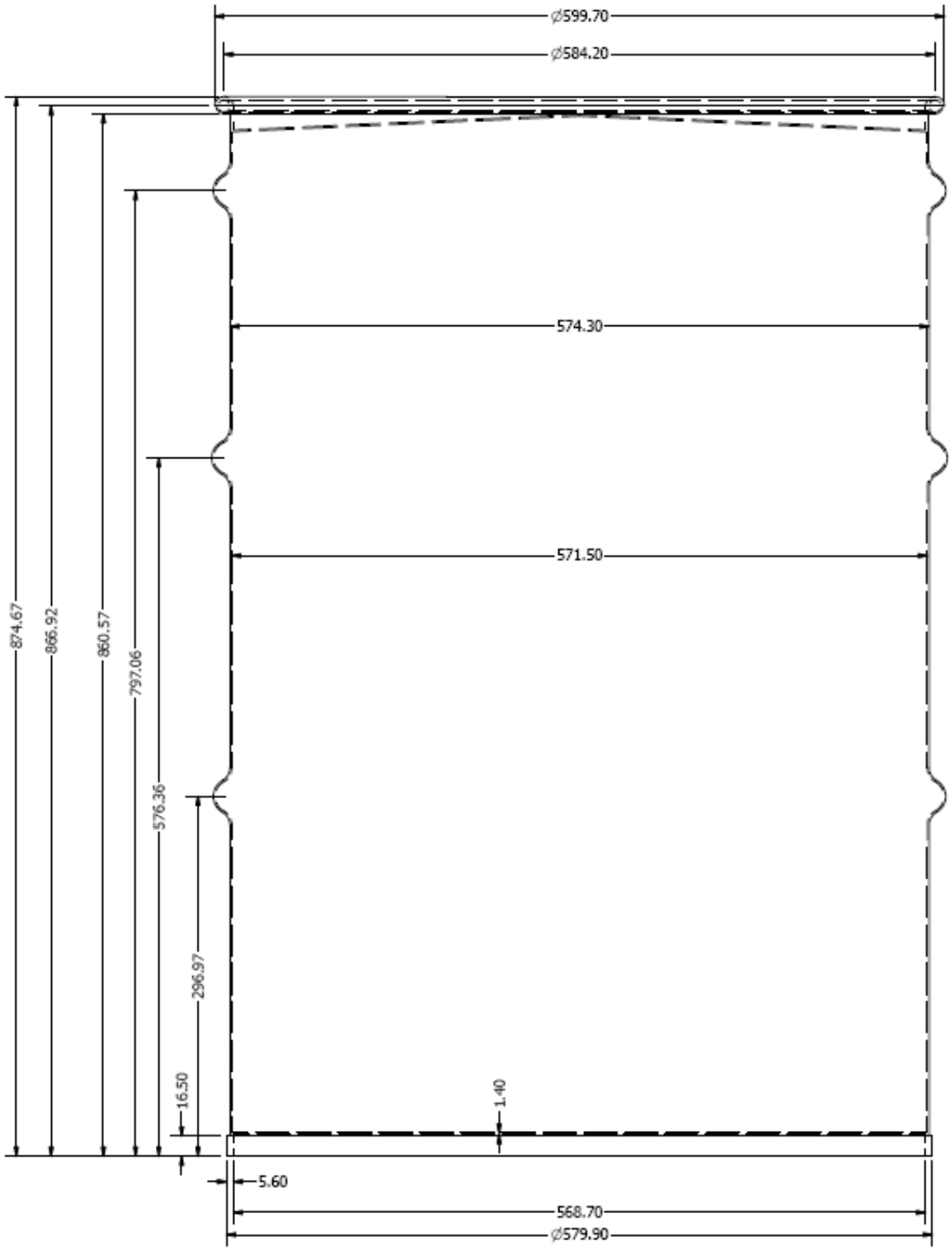

Figure A1: Drum

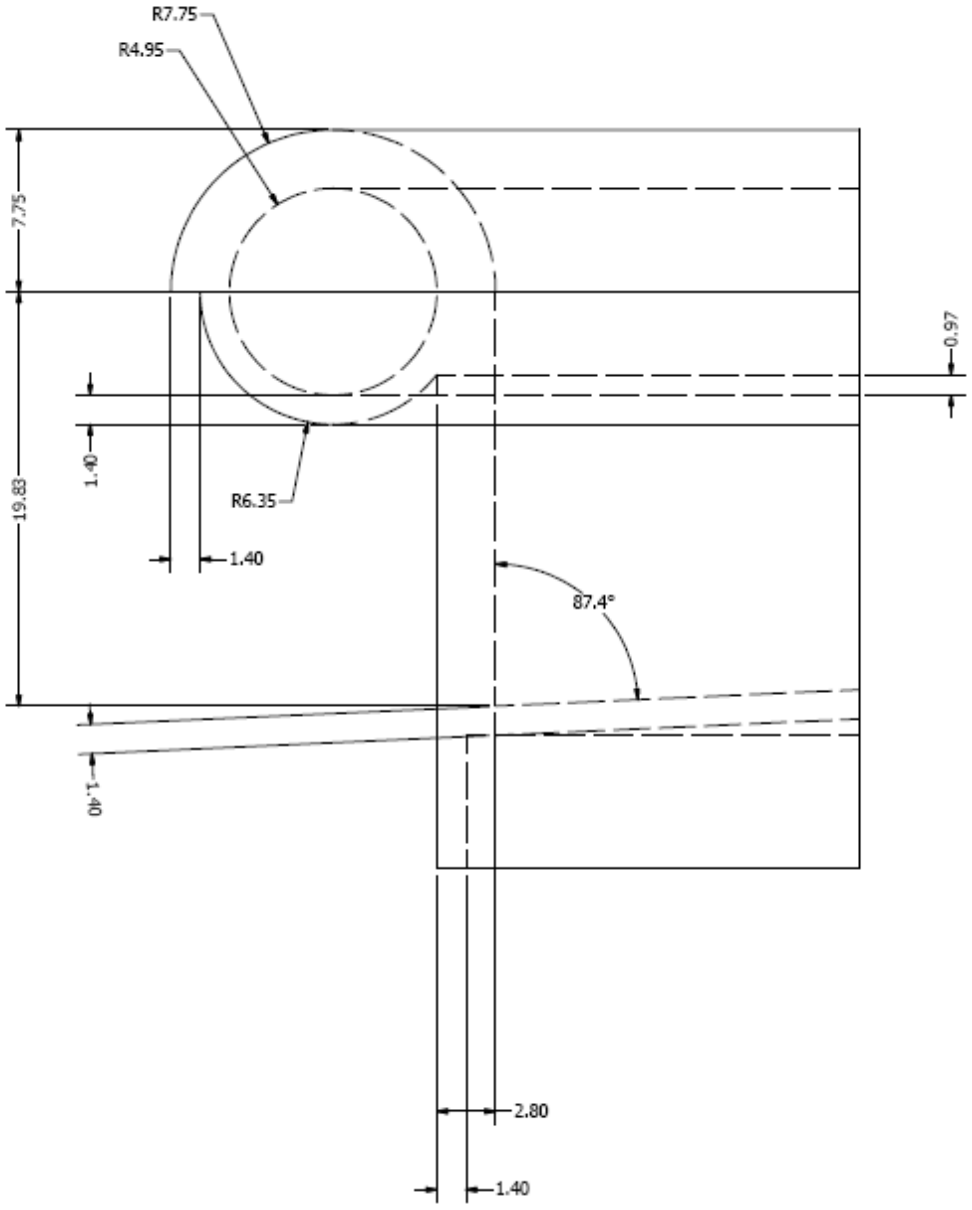

Figure A2: Top detail

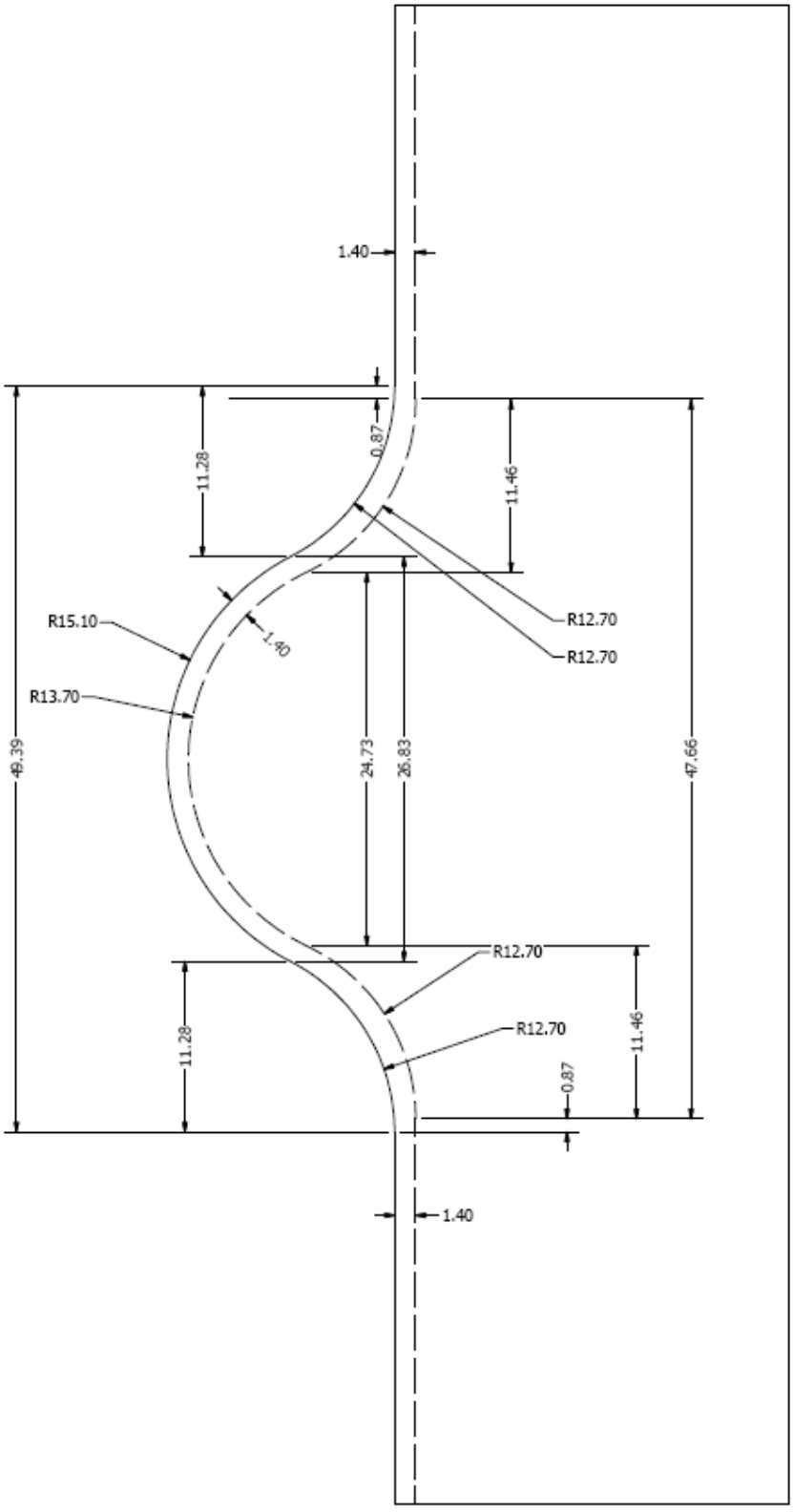

Figure A3: Side detail (Note that some dimensions were changed slightly in the MCNP input file to avoid geometry errors)

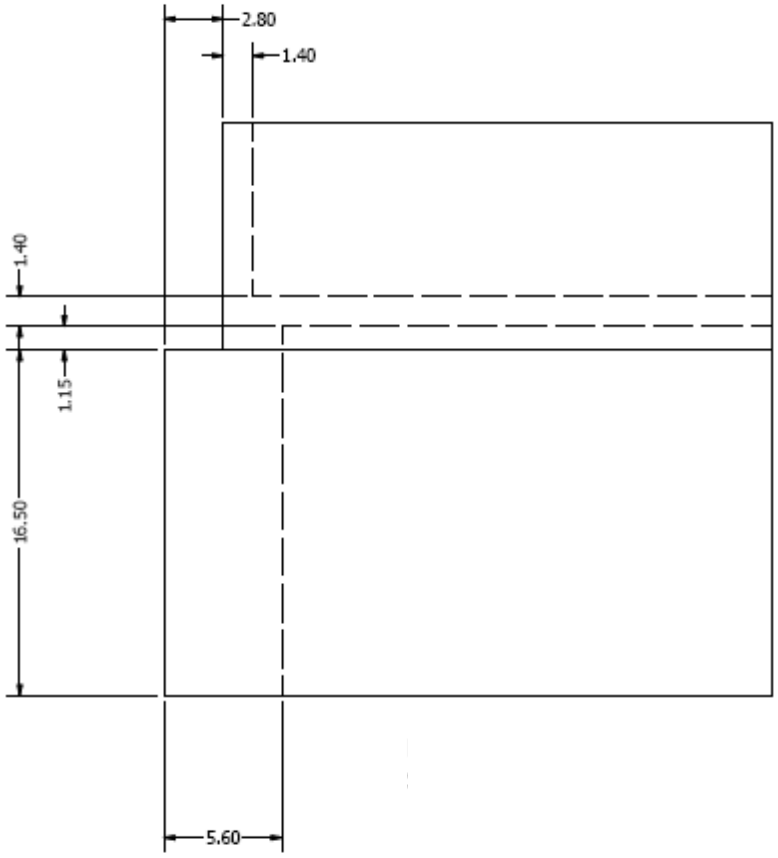

Figure A4: Bottom detail

App. B

MCNP Input

NOTE: This input file is for the drum with the overpack.
It includes the best estimate mixture at 0.2 g/cm^3 density.

```
Drum #24, best estimate, 0.2 g/cm^3, overpack
C --- cell cards ---
1000 1 -0.001292 -110 IMP:P=1
1010 2 -7.8 110 -111 301 -101 IMP:P=1
1020 2 -7.8 110 -112 101 -100 IMP:P=1
1030 2 -7.8 103 -101 -301 120 IMP:P=1
1040 2 -7.8 104 -103 -300 IMP:P=1
2000 2 -7.8 200 -201 120 -205 IMP:P=1
2010 2 -7.8 -301 120 201 -202 IMP:P=1
2020 2 -7.8 202 -203 -301 IMP:P=1
3000 2 -7.8 203 -340 300 -301 IMP:P=1
3010 2 -7.8 340 310 -311 -302 300 IMP:P=1
3020 2 -7.8 302 312 -313 IMP:P=1
3030 2 -7.8 -302 314 -315 -341 300 IMP:P=1
3040 2 -7.8 341 300 -301 -342 IMP:P=1
3050 2 -7.8 342 320 -321 -302 300 IMP:P=1
3060 2 -7.8 302 322 -323 IMP:P=1
3070 2 -7.8 -302 324 -325 -343 300 IMP:P=1
3080 2 -7.8 343 300 -301 -344 IMP:P=1
3090 2 -7.8 344 330 -331 -302 300 IMP:P=1
3100 2 -7.8 302 332 -333 IMP:P=1
3110 2 -7.8 -302 334 -335 -345 300 IMP:P=1
3120 2 -7.8 345 300 -301 -103 IMP:P=1
3300 3 -0.2 -104 203 -300 IMP:P=1
3320 3 -0.2 300 -312 IMP:P=1
3340 3 -0.2 -336 300 312 315 -302 311 -350 IMP:P=1
3350 3 -0.2 -336 300 312 315 -302 311 350 IMP:P=1
3370 3 -0.2 300 -322 IMP:P=1
3380 3 -0.2 -337 300 322 325 -302 321 -351 IMP:P=1
3390 3 -0.2 -337 300 322 325 -302 321 351 IMP:P=1
3410 3 -0.2 300 -332 IMP:P=1
3420 3 -0.2 -338 300 332 335 -302 331 -352 IMP:P=1
3430 3 -0.2 -338 300 332 335 -302 331 352 IMP:P=1
4000 1 -0.001292 -400 IMP:P=1
5000 1 -0.001292 702 -501 -510 IMP:P=1 $ air above
5010 1 -0.001292 500 -700 -510 IMP:P=1 $ air below
5011 1 -0.001292 600 -510 700 -702 400 IMP:P=1 $ air beside
5020 1 -0.001292 201 -101 302 112 313 323 333 -710 IMP:P=1
5022 1 -0.001292 -600 711 700 -702 IMP:P=1
5023 1 -0.001292 100 -701 -710 IMP:P=1
5030 1 -0.001292 200 -201 205 -710 IMP:P=1
5040 1 -0.001292 111 -112 301 -101 IMP:P=1
5050 1 -0.001292 -101 103 -120 IMP:P=1
5060 1 -0.001292 -100 101 112 -710 IMP:P=1
5070 1 -0.001292 -120 200 -202 IMP:P=1
5080 1 -0.001292 201 301 -302 310 -340 IMP:P=1
5090 1 -0.001292 -302 -310 IMP:P=1
5100 1 -0.001292 -302 -314 IMP:P=1
5110 1 -0.001292 341 -342 314 320 301 -302 IMP:P=1
5120 1 -0.001292 -302 -320 IMP:p=1
5130 1 -0.001292 -302 -324 IMP:P=1
5140 1 -0.001292 343 -344 324 330 301 -302 IMP:P=1
5150 1 -0.001292 -302 -330 IMP:P=1
```

```
5160 1 -0.001292 -302 -334 IMP:P=1
5170 1 -0.001292 345 -101 334 112 301 -302 IMP:P=1
7000 2 -7.8 -200 700 -711 IMP:P=1 $ overpack bottom
7010 2 -7.8 200 -701 710 -711 IMP:P=1 $ overpack sides
7020 2 -7.8 701 -702 -711 IMP:P=1 $ overpack top
9999 0  -500 :501 :510 IMP:P=0 $ the rest of the universe!

C --- surface cards ---
100 pz 87.467 $ planes for the top and lid
101 pz 86.692
103 pz 84.709 $ top of the lid
104 pz 84.569 $ bottom of the lid
110 tz 0 0 86.692 29.21 .495 .495 $ inside of lip
111 tz 0 0 86.692 29.21 .635 .635 $ outside of lip
112 tz 0 0 86.692 29.21 .775001 .775001 $ lid around lip
120 cz 28.435 $ inner part of the lid
200 pz 0 $ very bottom of the walls and drum
201 pz 1.65 $ top of the lip around the bottom edge
202 pz 1.765 $ bottom of the bottom panel
203 pz 1.905 $ top of the bottom panel
205 cz 28.995 $ outside of the bottom, beyond the drum walls
300 cz 28.575 $ inner wall
301 cz 28.715 $ outer wall
302 cz 29.2075
310 tz 0 0 27.3241 29.945 1.22999 1.22999
311 tz 0 0 27.3241 29.945 1.3705 1.3705
312 tz 0 0 29.697 28.575 1.3695 1.3695
313 tz 0 0 29.697 28.575 1.51 1.51
314 tz 0 0 32.0669 29.945 1.22999 1.22999
315 tz 0 0 32.0669 29.945 1.3705 1.3705
320 tz 0 0 55.2631 29.945 1.22999 1.22999
321 tz 0 0 55.2631 29.945 1.3705 1.3705
322 tz 0 0 57.636 28.575 1.3705 1.3705
323 tz 0 0 57.636 28.575 1.51 1.51
324 tz 0 0 60.0089 29.945 1.22999 1.22999
325 tz 0 0 60.0089 29.945 1.3705 1.3705
330 tz 0 0 77.3331 29.945 1.22999 1.22999
331 tz 0 0 77.3331 29.945 1.3705 1.3705
332 tz 0 0 79.706 28.575 1.3705 1.3705
333 tz 0 0 79.706 28.575 1.51 1.51
334 tz 0 0 82.0789 29.945 1.22999 1.22999
335 tz 0 0 82.0789 29.945 1.3705 1.3705
336 tz 0 0 29.697 28.575 2.3729 2.3729
337 tz 0 0 57.636 28.575 2.3729 2.3729
338 tz 0 0 79.706 28.575 2.3729 2.3729
340 pz 27.3241
341 pz 32.0669
342 pz 55.2631
343 pz 60.0089
344 pz 77.3331
345 pz 82.0789
350 pz 29.697
351 pz 57.636
352 pz 79.706
400 s 0 100 43.7335 2
500 pz -30
501 pz 100
510 cz 130
```

```
600 cz 50
610 pz 46.25
620 pz 53.75
700 pz -8.89
701 pz 88
702 pz 96.89
710 cz 31
711 cz 39.89

C --- data cards ---
vol 34j 1955.438 22j
m1 7000.04p 7.80642E-01 &
   8000.04p 2.09677E-01 &
   18000.04p 9.33764E-03 &
   6000.04p 3.15920E-04 &
   10000.04p 1.81754E-05 &
   2000.04p 5.23867E-06 &
   54000.04p 8.69771E-08 &
   1000.04p 2.49937E-08 $ Air based on 1976 USSA rho=-0.001292
m2 6000.04p 0.0020 &
   25000.04p 0.0090 &
   15000.04p 0.0004 &
   16000.04p 0.0005 &
   26000.04p .9881 $ 1018 Steel rho=-7.8
m3 1000.04p .6 &
   6000.04p .3 &
   8000.04p .1
mode p
sdef erg=0.662 par=p pos=0 0 50
nps 2e8
e0 0.00005 500I .665
f2:p 600
fs2 -200 -610 -620 -100
sd2 9424.778 14529.866 2356.194 10592.508 3937.358
f12:p 510
fs12 -200 -610 -620 -100
sd12 24504.423 37777.652 6126.106 27540.521 10237.131
f5z:p 50 50 7.5
f15z:p 50 130 7.5
f25z:p 25 50 7.5
```